



5-hydroxymethylfurfural as an important component of cigarette smoke impairs the blood-testis barrier via mTOR/Atg12-mediated autophagy in Sertoli cells in mice

Yongquan Yu^{a,b,c}, Liu Yang^{b,c}, Mengfan Peng^c, Shuyu Xu^{b,c}, Mingxiu Duan^c, Li Wang^c, Rong Xia^c, Lifeng Tan^{d,*}, Shushu Li^{d,e,**}, Shou-Lin Wang^{b,c,***} 

^a Key Lab of Environmental Medicine Engineering of Ministry of Education, School of Public Health, Southeast University, Nanjing, China

^b State Key Lab of Reproductive Medicine and Offspring Development, Institute of Toxicology, Nanjing Medical University, Nanjing, China

^c Key Lab of Modern Toxicology of Ministry of Education, Center for Global Health, School of Public Health, Nanjing Medical University, Nanjing, China

^d Changzhou Center for Disease Control and Prevention, Changzhou Medical Center, Nanjing Medical University, Changzhou, China

^e Nanjing Women and Children's Healthcare Hospital, Women's Hospital of Nanjing Medical University, Nanjing, China

ARTICLE INFO

Keywords:

Cigarette smoke
5-hydroxymethylfurfural
Blood–testis barrier
Autophagy
Atg12

ABSTRACT

Cigarette smoke, an indoor environmental pollutant, poses a major threat to male reproductive health worldwide, yet its complex composition has hindered the identification of the important toxic components responsible for this damage. We previously identified 5-hydroxymethylfurfural (5-HMF) as an abundant toxic component of cigarette smoke extract (CSE), but its role and mechanism in spermatogenesis remain unclear. In this study, we first identified a positive correlation between serum levels of 5-HMF and those of nicotine and cotinine in a community-based cross-sectional study in Jiangsu province, China. We then exposed male C57BL/6 mice to aerosolized CSE, 5-HMF-enriched fraction of CSE (CSE-HMF), or pure 5-HMF for 60 days. The results showed that 5-HMF appeared in blood and testis of mice. Both CSE-HMF and pure 5-HMF recapitulated the reproductive damage observed with CSE, significantly impairing testicular morphology and spermatogenesis without altering sex hormone levels. Furthermore, 5-HMF penetrated the testis and disrupted the blood-testis barrier (BTB), compromising its function and reducing transepithelial electrical resistance (TER) in Sertoli cells. These impairments were driven by increased autophagic flux and subsequent downregulation of tight junction (TJ) proteins, which was prevented by autophagy inhibitors. Mechanistically, 5-HMF decreased p-mTOR and up-regulated Atg12 to stimulate autophagic flux in testis and Sertoli cells. Heterozygous deficiency of Atg12 (*atg12^{+/-}*) significantly attenuated 5-HMF-induced autophagy activation, BTB disruption, and spermatogenic impairment. Our work identifies 5-HMF as one of the important toxic components of cigarette smoke that impairs spermatogenesis by triggering mTOR/Atg12-dependent autophagy, which disrupts TJs between Sertoli cells and consequently compromises the BTB.

1. Introduction

Cigarette smoking remains a major global public health challenge, with an estimated 20 % of adults worldwide consuming tobacco products (Rigotti et al., 2022). The resulting emission of particulate matter and harmful chemicals from cigarettes poses a significant risk to both users and bystanders, making it a leading cause of indoor environmental

pollution (Radbel et al., 2024). Moreover, cigarette smoking is a well-established risk factor for a broad spectrum of chronic diseases, including respiratory, cardiovascular, and reproductive disorders (Gutvirtz and Sheiner, 2022). The association with male infertility is particularly critical, given that male factors are the primary cause of infertility in 20–30 % of cases and a contributory cause in 50–60 % of couples, affecting approximately 186 million people worldwide (Rahban

* Corresponding author.

** Corresponding author at: Shushu Li, Nanjing Women and Children's Healthcare Hospital, Women's Hospital of Nanjing Medical University, Nanjing, China.

*** Corresponding author at: Shou-Lin Wang, Key Lab of Modern Toxicology of Ministry of Education, Center for Global Health, School of Public Health, Nanjing Medical University, Nanjing, China.

E-mail addresses: cztanlifeng@163.com (L. Tan), lishushu@njmu.edu.cn (S. Li), wangshl@njmu.edu.cn (S.-L. Wang).

<https://doi.org/10.1016/j.ecoenv.2026.119825>

Received 8 November 2025; Received in revised form 21 January 2026; Accepted 1 February 2026

Available online 4 February 2026

0147-6513/© 2026 The Author(s). Published by Elsevier Inc. This is an open access article under the CC BY-NC license (<http://creativecommons.org/licenses/by-nc/4.0/>).

and Nef, 2020; Rotimi and Singh, 2024). Indeed, robust epidemiological evidence has linked smoking to impaired sperm quality, including lower count, reduced motility, and aberrant morphology (Boeri et al., 2019; Sharma et al., 2016), which is further supported by experimental studies (Esakky et al., 2018; La Maestra et al., 2015). However, as cigarette smoke is a highly complex mixture capable of damaging reproductive tissues, identification of its important reproductive toxicants is crucial for elucidating the mechanisms of male reproductive damage. 5-hydroxymethylfurfural (5-HMF) is a furan compound generated via the Maillard reaction during the heating or combustion of carbohydrates (Aktağ and Gökmen, 2021). Since carbohydrates are present not only in foods but also in natural materials, such as tobacco leaves, straw, and wood, 5-HMF is widely found in the smoke produced from these sources, including cigarette smoke, wood smoke, and smoke from burning straw (Hermundsgård et al., 2025; Karlsson et al., 2012). It was first identified in cigarette smoke extract (CSE) in our previous study (Ji et al., 2018). We quantified that the content of 5-HMF in cigarette smoke was 2.01 ± 0.04 mg/cigarette, which is comparable to that of nicotine (0.75–2.49 mg/cigarette) (Bao et al., 2010) and nearly four orders of magnitude greater than that of NNK (1.59–7.22 ng/cigarette) (Zhang et al., 2016), establishing 5-HMF as a predominant toxicant in cigarette smoke. Meanwhile, recent studies reported that 5-HMF can increase testicular oxidative stress and apoptosis, induce seminiferous tubule atrophy and epithelial degeneration, and decrease sperm count in mice (Aydin et al., 2025; Orta Yilmaz and Aydin, 2024). Therefore, we speculate that 5-HMF may play a critical role in cigarette smoke-induced testicular toxicity, a mechanism that remains to be elucidated.

Spermatogenesis is a precisely regulated process that leads to the production of mature sperm. During germ cell development, the blood-testis barrier (BTB) plays an indispensable role by protecting meiotic and postmeiotic germ cells from immunological molecules, pathogens, and toxicants in the circulation (Mruk and Cheng, 2015). Pathologically, exposure to reproductive toxicants can disrupt BTB function, thereby not only compromising the testicular immunoprivileged microenvironment but also facilitating the entry of additional toxicants into the testes, which further exacerbates testicular damage (Zheng et al., 2024). For instance, oral exposure to deoxynivalenol (DON) has been shown to disrupt the BTB, aggravate testicular inflammation, and ultimately lead to reproductive disorders (Cao et al., 2020). Similarly, perfluorooctane sulfonate (PFOS) compromises murine spermatogenesis by targeting Sertoli cells and BTB integrity, which allows increased PFOS permeation into the testes where it directly disrupts spermatogenesis (Qiu et al., 2013). Therefore, the BTB and its constituent Sertoli cells, located in the basal compartment of the seminiferous tubules, may serve as early targets for exogenous toxicants and play a critical role in resulting reproductive dysfunction (Jiang et al., 2024a).

The BTB is a composite structure consisting of tight junctions (TJs), ectoplasmic specializations (ESs), desmosomes, and gap junctions (GJs) between adjacent Sertoli cells (Cheng and Mruk, 2012). The assembly of these junction proteins into a structural complex is essential for BTB integrity and function, and the reduced expression of junction proteins such as ZO-1, Claudin-5, and Connexin 43, is a primary mechanism leading to BTB disruption (Peña-Corona et al., 2023). While the canonical endosome-lysosome pathway has been the focus of BTB regulation research, recent work has demonstrated that macroautophagy (autophagy), a lysosomal degradation process mediated by autophagy-related (ATG) proteins and signaling pathways, also plays a key regulatory role, particularly in the context of xenobiotic insult (Jiang et al., 2024b; Yan et al., 2022). As reported, glyphosate induced the autophagic degradation of Connexin 43 in the testis by directly interacting with ER- α , resulting in BTB disruption in roosters (Liang et al., 2024). Moreover, PI3K/AKT/mTOR-mediated autophagy in Sertoli cells was reported to be a key mechanism through which PFOS compromised BTB integrity (Chen et al., 2024b). Consequently, inhibiting autophagy has emerged as a promising therapeutic strategy for counteracting xenobiotic-induced BTB damage (Wang et al., 2025). Of

note, a recent study demonstrated that 5-HMF activates autophagy in cardiomyocytes and mediates doxorubicin-induced myocardial injury in mice (Wu et al., 2025). We further hypothesize that 5-HMF might distribute to the testis and disrupt spermatogenesis by compromising BTB integrity through the regulation of autophagy.

In this study, the association between serum levels of nicotine, cotinine, and 5-HMF was first examined in participants from a community-based cross-sectional study in Jiangsu province, China, to provide human data linking 5-HMF to smoking exposure. Subsequently, mouse exposure models were established using CSE, 5-HMF-enriched fraction of CSE (CSE-HMF), or pure 5-HMF, and a comprehensive assessment was conducted to evaluate 5-HMF levels in serum and testis, its effects on spermatogenesis and the BTB, and the underlying autophagy-related mechanism. These mechanistic insights were further validated using *atg12* haploinsufficient (*atg12*^{+/-}) mice. Our findings should provide novel insights into the toxicological effects of 5-HMF as a predominant cigarette smoke toxicant on spermatogenesis and underscore the critical role of autophagy in BTB disruption.

2. Materials and methods

2.1. Study population

Male participants were recruited from a community-based, cross-sectional study conducted in Jiangsu province, China, as previously described (Li et al., 2025b). Upon enrollment, each participant completed a comprehensive assessment consisting of a physical examination, blood draw for serum isolation, and a standardized interview. The questionnaire collected information on demographic characteristics, lifestyle factors (including smoking status), and dietary habits. All procedures were performed by trained health professionals. After excluding subjects with missing data on serum 5-HMF, nicotine or cotinine, 885 male participants who had been enrolled from June 2019 to December 2020 were included in the analysis. The study protocol was approved by the Institutional Review Board of the Changzhou Centers for Disease Control and Prevention (Approval No.: Changzhou CDC Ethics [2019] 01), and all participants provided written informed consent prior to participation.

2.2. Preparation of CSE and isolation of the 5-HMF-enriched fraction

The cigarette smoke sampling apparatus consisted of a constant-flow air sampler, a glass impinger (charged with 10 mL of chloroform as the absorption solution), and a cigarette, connected in sequence with rubber tubing. Smoking was conducted at a flow rate of 75 mL/min, which allowed each cigarette to be consumed uniformly within 5 min. A total of one pack (20 cigarettes) was smoked per replicate. The chloroform solution was then evaporated under a nitrogen stream, and the dry residue was reconstituted in 1 mL of chloroform to obtain the CSE. Subsequently, the content of 5-HMF in the CSE was quantified using high-performance liquid chromatography with an ultraviolet detector (HPLC-UV). The analysis was carried out on an Eclipse XDB-C18 column (4.6 × 250 mm, 5 μ m) with an injection volume of 20 μ L. The detection wavelength was set at 284 nm, and 5-HMF had a retention time of 7.35 min.

To isolate the 5-HMF-enriched fraction (HMF-CSE), the CSE in chloroform was extracted with an equal volume of deionized water. The aqueous layer was collected after phase separation, and the extraction was repeated with a fresh portion of water. The combined aqueous extracts were filtered through a 0.45 μ m aqueous filter and then subjected to fractionation on a Sephadex LH-20 column to collect the target fraction.

2.3. Animals and 5-HMF exposure models

Pathogen-free male wild-type (WT) C57BL/6 mice were purchased

from the Animal Core Facility of Nanjing Medical University. *atg12*^{+/−} mice on a C57BL/6 background were generated by the Model Animal Research Center of Nanjing University using the CRISPR-Cas9 method. The F0 mice were subsequently backcrossed for at least five generations to stabilize the genetic background. All animals were maintained under

specific pathogen-free (SPF) conditions with a 12-h/12-h light/dark cycle at a controlled ambient temperature of $25 \pm 1^\circ\text{C}$. Mice were housed in individually ventilated cages and provided with food and tap water *ad libitum*. All experimental procedures were approved by the Animal Care and Welfare Committee of Nanjing Medical University

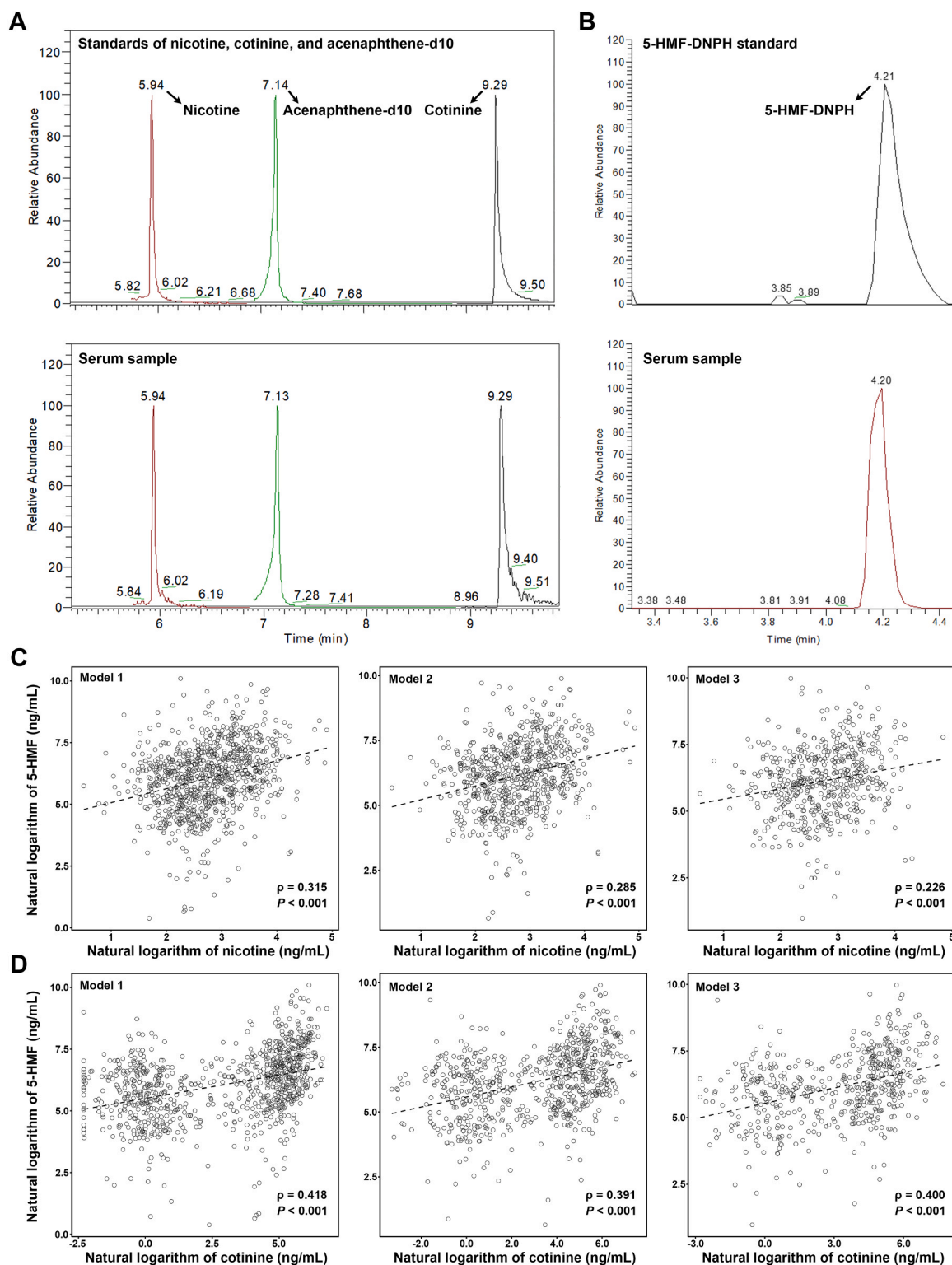


Fig. 1. Association between cigarette smoking and serum 5-HMF levels. (A) GC-MS/MS chromatograms of a standard mixture (nicotine, cotinine, and acenaphthene-d10) and a representative serum sample. (B) LC-MS chromatograms of 5-HMF-DNPH standard and a representative serum sample. (C-D) Partial correlations between serum levels of log-transformed 5-HMF and nicotine (C) or cotinine (D) in subjects included in this study. Model 1 was unadjusted. Model 2 was adjusted for age, BMI, education level, occupation, monthly household income. Model 3 was further adjusted for dietary intake based on model 2.

(IACUC-1811058) and conducted in accordance with institutional guidelines.

After one week of acclimation, 10–12-week-old male mice were used for the 5-HMF exposure experiments based on comparable age and body weight. (1) To determine the role of 5-HMF in cigarette smoke-induced spermatogenesis disruption, WT mice ($n = 6$ per group) were subjected to nose-only aerosol exposures for 60 days (6 days/week, 20 min per day) using a computer-assisted system (YLS-8B, Yiyan Technology, China), covering two full spermatogenic cycles. The exposure groups were as follows: saline (vehicle control), CSE (prepared from 20 cigarettes and dissolved in 20 mL saline), or CSE-HMF. (2) To investigate 5-HMF-induced BTB disruption and autophagy dysfunction, WT mice ($n = 7$ per group) were exposed to aerosols of either saline or 5-HMF (F065253, J&K Scientific Ltd., China; 2 mg/mL in 20 mL saline) using the same nose-only system and daily exposure duration (20 min). The daily dose for CSE, CSE-HMF, and pure 5-HMF treatments was set to correspond to smoke from 20 cigarettes (approximately one pack per day). This dose represents the typical exposure level of heavy smokers, as defined in epidemiological studies and linked to significantly elevated risks of multiple diseases, including male infertility (De Brucker et al., 2025; Kulaksiz et al., 2022). Accordingly, the design simulates sustained human exposure to assess its potential to induce the reproductive toxicity under investigation. (3) To determine the role of autophagy in 5-HMF-induced BTB disruption, WT and *atg12*^{+/-} mice were randomly assigned to four groups ($n = 6$ per group): WT + Saline group, WT + pure 5-HMF group, *atg12*^{+/-} + Saline group and *atg12*^{+/-} + pure 5-HMF group. The exposure protocol was identical to that used in experiment (2). Throughout the study, all mice were monitored daily and weighed every three days. At the experimental endpoint, mice were euthanized by cervical dislocation. Testes, epididymides, and blood samples were collected for subsequent analysis.

2.4. Measurement of nicotine, cotinine and 5-HMF in serum and testis

Serum nicotine and cotinine levels were quantified by gas chromatography-tandem mass spectrometry (GC-MS/MS) with acenaphthene-d10 (254320, J&K Scientific Ltd., China) employed as the internal standard (Fig. 1A). Briefly, an aliquot of 50 μ L serum was mixed with 50 μ L of acenaphthene-d10 (0.2 μ g/mL) and 100 μ L of methanol to precipitate proteins. After vortex mixing for 30 s, the mixture was centrifuged at $12,000 \times g$ for 20 min at 4°C. The resulting supernatant was then subjected to instrumental analysis. Chromatographic separation was achieved using a DB-EUPAH capillary column (20 m \times 0.18 mm, 0.14 μ m) with helium as the carrier gas at a constant flow rate of 1.0 mL/min. The GC temperature program was initialized at 60°C (held for 1 min), ramped to 280°C at a rate of 20°C/min, and finally held at 280°C for 2 min. Analysis was performed in multiple reaction monitoring (MRM) mode, monitoring the following quantitative ion transitions: m/z 162.2 \rightarrow 84.1 for nicotine and m/z 176.2 \rightarrow 98.1 for cotinine. The limit of detection (LOD) was 0.1 ng/mL for nicotine and 0.2 ng/mL for cotinine. The mean spiked recoveries were 84.9–120.6 %, with relative standard deviations (RSDs) of 2.0–12.3 % ($n = 3$). Values below the LOD were imputed as the LOD divided by the square root of 2.

5-HMF levels in serum and testis were quantified using liquid chromatography-mass spectrometry (LC-MS) with ¹³C-5-HMF (H947002, Toronto Research Chemicals Co., Ltd., Canada) as the internal standard (Fig. 1B). Briefly, 20 μ L of serum or testicular homogenate was spiked with 10 μ L of ¹³C-5-HMF (0.5 μ g/mL) and 30 μ L of methanol for protein precipitation. The mixture was vortexed, kept in the dark for 5 min, and then centrifuged ($12,000 \times g$, 10 min, 4°C). The resulting supernatant was transferred to a new tube and reacted with 40 μ L of 20 mM 2,4-dinitrophenylhydrazine (DNPH) at 37°C for 60 min with shaking. The reaction was quenched by adding 24 μ L of 0.5 M potassium hydroxide (KOH), followed by centrifugation ($12,000 \times g$, 15 min, 4°C). The final supernatant (10 μ L) was injected into the LC-MS system. Separation was achieved using a BEH Shield RP18 column

maintained at 35°C. Mobile phase A was water with 0.1 % formic acid, and mobile phase B was acetonitrile with 0.1 % formic acid, at a flow rate of 0.3 mL/min. The quantitative ion transition was m/z 307.06 \rightarrow m/z 289.0592. The LOD was 2.0 ng/mL. The mean spiked recoveries were 98.3–106.1 %, with RSDs of 2.2–4.5 % ($n = 3$). Values below the LOD were imputed as the LOD divided by the square root of 2.

2.5. Computer-assisted sperm analysis (CASA)

The freshly dissected cauda epididymis was rinsed three times with PBS (37°C) and then minced using fine scissors. Spermatozoa were released into M199 medium and incubated at 37°C for 5 min. Sperm count and motility were evaluated using a CASA system (Hamilton Thorne, USA). Aliquots of 20 μ L sperm suspension were placed on pre-warmed glass slides maintained at 37°C and immediately examined under 400 \times magnification. For each sample, 10 images were captured and analyzed using the corresponding software.

2.6. Histopathological analysis

The testicular and epididymal tissues were rinsed three times with PBS and fixed in Davidson's fixative solution for 24 h. Subsequently, the tissues were routinely processed through dehydration, embedded in paraffin, sectioned at a thickness of 5 μ m, and stained with hematoxylin and eosin (H&E) following the manufacturer's instructions. Digital images were acquired using a Panoramic MIDI scanner (3DHISTECH, Hungary).

2.7. Measurement of serum sex hormone levels

Serum concentrations of testosterone (T), estradiol (E₂), follicle-stimulating hormone (FSH), and luteinizing hormone (LH) were measured using commercially available enzyme-linked immunosorbent assay (ELISA) kits (JiYinMei Bioscience, China) according to the manufacturer's instructions. Aliquots of 80 μ L serum were diluted and analyzed accordingly. Absorbance readings were obtained using a TECAN Infinite 200 PRO microplate reader (Tecan, Switzerland).

2.8. Measurement of BTB permeability in vivo

The integrity of the BTB was assessed according to previous study (Xia et al., 2023). Briefly, the biotin tracer EZ-Link Sulfo-NHS-LC-Biotin (21335, Thermo Fisher Scientific, USA), prepared in sterile PBS supplemented with 1 mM CaCl₂, was administered via intratesticular injection (50 μ L) to the right testis of mouse, and allowed to diffuse for 30 min. The testis was then immersed in Tissue-Tek OCT compound (Sakura Finetek, Japan) and sectioned at 10 μ m thickness using a cryostat microtome (Thermo Fisher Scientific, USA). The tissue sections were fixed in a 1:1 mixture of methanol and acetone, blocked with 5 % BSA and 0.1 % Triton X-100 in 0.1 M PBS, and incubated with Alexa Fluor® 647-conjugated streptavidin at 37°C for 1 h. Fluorescence imaging was performed using a Carl Zeiss LSM700 confocal microscope (Jena, Germany).

2.9. Cell isolation, culture and treatment of 5-HMF

Primary Sertoli cells were isolated from 14-day-old male WT or *atg12*^{+/-} C57BL/6 mice as described previously (Saewu et al., 2020). Briefly, decapsulated testicular tissues were rinsed with ice-cold PBS and minced into small fragments. The fragments were subjected to enzymatic digestion using a trypsin solution (1 mg/mL containing 5 μ g/mL DNase I) at 37°C for 5 min. The cell pellet was further incubated in Ham's F12 and Dulbecco's Modified Eagle's Medium (DMEM/F12) supplemented with 0.5 mg/mL collagenase, 1 mg/mL hyaluronidase, and 5 μ g/mL DNase I at 37°C for 30 min. Sertoli cells were further purified through hypotonic treatment with 20 mM Tris (pH 7.4) at 22°C.

The cells were maintained in DMEM/F12 culture medium containing 10 µg/mL insulin, 5 µg/mL human transferrin, 5 µg/mL bacitracin, and 2.5 ng/mL epidermal growth factor. Sertoli cell identity was confirmed using the marker protein WT-1.

In the exposure experiment, Sertoli cells were treated with 5-HMF (10–40 µM) or vehicle control (DMSO) for 24 h. The autophagy inhibitors chloroquine diphosphate salt (CQ, C6628, Sigma-Aldrich Corp., USA) and 3-methyladenine (3-MA, HY-19312, MedChem Express, USA) were applied at concentrations of 20 µM and 1 mM, respectively.

2.10. Measurement of BTB permeability in vitro

Isolated Sertoli cells were seeded as monolayers at a density of 1×10^6 cells/cm² on Matrigel-coated bicameral chambers (Millipore, USA). Transepithelial electrical resistance (TER) was measured at four equidistant locations (corresponding to the 12, 3, 6, and 9 o'clock positions) within each unit. These values were averaged to obtain R_{sample} . Blank control units (without cells) were measured in parallel to determine R_{blank} . The true TER value for each sample was calculated based on the formula:

$$\text{TER}_{\text{sample}} (\Omega \cdot \text{cm}^2) = (R_{\text{sample}} - R_{\text{blank}}) (\Omega) \times \text{Effective Membrane Area (cm}^2\text{)}.$$

TER measurements were initiated 24 h after plating, and the culture medium was replaced daily. Based on established protocols, a functional barrier was considered formed by day 4, at which point the indicated treatments were applied individually or in combination to the lower chamber. Experiments were performed in three independent replicates.

2.11. Cell transfection with lentivirus

Due to the limited transfection efficiency of isolated Sertoli cells, the mouse Sertoli cell line TM4 was used for transfection with LC3-GFP-mRFP lentivirus (Hanbio, China) to analyze autophagy flux. TM4 cells were purchased from Shanghai Institute of Biochemistry and Cell Biology (Chinese Academy of Sciences, China) and routinely tested to confirm the absence of mycoplasma contamination. Cells were cultured in DMEM/F12 medium supplemented with 2.5 % fetal bovine serum (FBS), 5 % horse serum (HS) and 1 % penicillin-streptomycin at 37 °C with 5 % CO₂ and 95 % humidity.

For transfection, TM4 cells were plated in 24-well plates and cultured until reaching 45–55 % confluence. Lentiviral particles were diluted in Opti-MEM containing 8 µg/mL polybrene to a multiplicity of infection (MOI) of 30 and then applied to the cells for 24 h. After incubation, the viral medium was replaced with fresh complete medium containing 3 µg/mL puromycin to select for stably transduced cells. After experimental treatments, cells were fixed with 4 % paraformaldehyde at room temperature for 90 min and nuclei were labeled with DAPI for 15 min. Fluorescence imaging was performed using a Carl Zeiss LSM700 confocal microscope (Jena, Germany).

2.12. Immunofluorescence assay

Isolated Sertoli cells were seeded on confocal dishes and fixed with 4 % paraformaldehyde at room temperature for 90 min. After three PBS washes, the cells were incubated with QuickBlock™ blocking buffer for 60 min. The samples were then incubated overnight at 4°C with the following primary antibodies: WT-1 (12609-1-AP, Proteintech, USA), LC3 (4108, Cell Signaling Technology, USA), and Occludin (33-1500, Thermo Fisher Scientific, USA). This was followed by incubation with appropriate fluorescent secondary antibodies at 37°C for 60 min. Nuclei were stained with DAPI for 15 min. Fluorescence imaging was performed using a Carl Zeiss LSM700 confocal microscope (Jena, Germany). Experiments were performed in three independent replicates.

2.13. Transmission electron microscopy (TEM) analysis

Testicular tissues and isolated Sertoli cells were fixed in 2.5 % glutaraldehyde at 4°C for 24 h. The samples were then post-fixed in 1 % osmium tetroxide, followed by dehydration in a graded ethanol series (50 %–100 %) and propylene oxide, before being embedded in resin. Ultrathin sections were prepared and stained with uranyl acetate and lead citrate. The ultrastructural morphology of the testis and Sertoli cells was examined using a TEM (JEOL, Japan). Experiments were performed in three independent replicates.

2.14. Western blot analysis

Testicular tissues and isolated Sertoli cells were homogenized by sonication and lysed on ice for 30 min using RIPA buffer. Protein concentrations were determined with a BCA assay kit, followed by denaturation at 100°C for 15 min. Equal amounts of proteins (50–100 µg) were subsequently separated by sodium dodecyl sulfate–polyacrylamide gel electrophoresis (SDS-PAGE) and transferred onto polyvinylidene fluoride (PVDF) membranes. After blocking with 5 % bovine serum albumin (BSA) for 60 min at room temperature, the membranes were incubated overnight at 4°C with specific primary antibodies. Immune complexes were detected using the ECL immunoblotting assay kit, with GAPDH serving as the loading control. Protein band intensities were quantified by densitometry using ImageJ software. The antibodies utilized are listed in Table S1. Experiments were performed in three independent replicates.

2.15. qRT-PCR analysis

RNA from testicular tissues was extracted with TRIzol reagent and reverse-transcribed into complementary DNA (cDNA) using HiScript II qRT SuperMix (Vazyme, China). The cDNA products were subsequently amplified with ChamQ SYBR qPCR Master Mix (Vazyme, China) on a LightCycler real-time PCR system (Roche, Switzerland) under the following conditions: initial activation at 95°C for 30 s, followed by 40 cycles of denaturation at 95°C for 10 s and annealing at 60°C for 30 s. Gene-specific primer sequences are listed in Table S2. Experiments were performed in three independent replicates.

2.16. Statistical analysis

For observational data, continuous variables were summarized as mean ± SD or median (IQR), while categorical variables were expressed as number (percentage). The levels of 5-HMF, nicotine and cotinine were natural log-transformed to approximate normal distribution prior to statistical analysis. The relationship between serum 5-HMF and smoking-related biomarkers (nicotine, cotinine) was assessed using partial correlation analysis with three sequential models. Model 1 was unadjusted. Model 2 controlled for age, BMI, education, occupation, and income. Model 3 additionally adjusted for dietary intake, including rice, wheat, vegetables, fruits, poultry, meat, eggs, fish, soybeans, dairy, fried food, preserved food, coffee, and sugary drinks. Differences in continuous variables between smokers and non-smokers were assessed using the Student's *t*-test or Mann–Whitney *U* test, while categorical variables were compared using the Chi-square test or Fisher's exact test. The *P*-value for trend was calculated using a general linear model to test for a linear association between smoking exposure and outcome indicators. The analyses were conducted with R software (version 4.1.2).

For experimental data, results are shown as mean ± SD. Differences between two groups were assessed using the independent-samples *t*-test, whereas comparisons among multiple groups were analyzed by one-way analysis of variance (ANOVA), followed by least significant difference post hoc tests. A *P*-value < 0.05 was considered statistically significant. The analyses were performed with SPSS 17.0 software.

3. Results

3.1. Serum 5-HMF levels are closely associated with cigarette smoking

The demographic characteristics of the study participants were presented in Table S3. The analysis included a total of 885 male individuals, with an average age of 51.74 ± 15.33 years. The proportions of workers/farmers, alcohol drinkers, and cigarette smokers were 25.99 %, 44.41 %, and 58.98 %, respectively. The median BMI was 25.16 kg/m², and median serum levels of 5-HMF, nicotine, and cotinine were 462.36 ng/mL, 15.25 ng/mL, and 55.40 ng/mL, respectively. Notably, daily intake of major food and drink groups (e.g., fried food, preserved food, meat, soybeans, coffee, and sugary drinks) did not differ significantly between smokers and non-smokers. In contrast, significant differences were observed in BMI, education level, and alcohol consumption between these two groups. Smokers exhibited significantly higher serum levels of 5-HMF, nicotine, and cotinine compared to non-smokers.

Moreover, as shown in Table 1, serum levels of 5-HMF, nicotine, and cotinine increased significantly with higher values of smoking intensity indicators, including smoking duration, daily cigarette consumption, and the Brinkman Index. Correlation analyses revealed significant positive correlations of serum 5-HMF with both nicotine and cotinine across all adjustment models. For nicotine (Fig. 1C), the partial correlation coefficients were $\rho = 0.315$ (Model 1, unadjusted), $\rho = 0.285$ (Model 2, adjusted for demographics and socioeconomic status), and $\rho = 0.226$ (Model 3, with further adjustment for dietary intake). For cotinine (Fig. 1D), the corresponding values were $\rho = 0.418$, 0.391, and 0.400,

Table 1

Serum levels of 5-HMF, nicotine and cotinine in populations with different smoking status.

	5-HMF, ng/mL	Nicotine, ng/mL	Cotinine, ng/mL
Smoking duration			
Non-smokers	275.86 (110.46, 592.90)	9.68 (7.17, 13.14)	0.94 (0.50, 1.83)
< 20 years	574.70 (229.65, 1419.87)	20.86 (14.92, 30.13)	137.29 (58.01, 250.89)
≥ 20 years	689.55 (290.46, 1473.57)	23.00 (14.92, 34.22)	172.06 (95.76, 267.70)
P for treand†	< 0.001	< 0.001	< 0.001
Smoking intensity ^a			
Non-smokers	275.86 (110.46, 592.90)	9.68 (7.17, 13.14)	0.94 (0.50, 1.83)
< 20 cigarettes/day	577.52 (233.64, 1359.74)	19.73 (12.97, 29.89)	131.47 (54.61, 214.35)
≥ 20 cigarettes/day	726.20 (302.42, 1571.87)	24.81 (16.52, 36.91)	201.27 (127.27, 302.99)
P for treand†	< 0.001	< 0.001	< 0.001
Brinkman Index ^b			
Non-smokers	275.86 (110.46, 592.90)	9.68 (7.17, 13.14)	0.94 (0.50, 1.83)
< 400	596.63 (236.36, 1390.92)	20.14 (13.99, 30.24)	132.89 (55.09, 231.87)
400–799	711.48 (369.28, 1596.95)	23.98 (15.89, 37.42)	183.89 (127.28, 302.18)
≥ 800	703.80 (258.90, 1333.29)	24.59 (16.12, 33.5)	185.37 (106.01, 264.37)
P for treand†	< 0.001	< 0.001	< 0.001

5-HMF, 5-Hydroxymethylfurfural; IQR, interquartile range.

Data are expressed as median (IQR).

^a The smoking intensity was categorized according to the number of cigarettes smoked per day.

^b The Brinkman Index was calculated as the smoking intensity multiplied by the smoking duration (in years).

† The P value for trend was calculated using a general linear model to test for a linear association between smoking exposure and the outcome indicators.

respectively. These results indicate that serum 5-HMF levels are associated with cigarette smoking, suggesting that cigarette smoke is a significant source of 5-HMF exposure in this population.

3.2. 5-HMF as an important component in cigarette smoke induces male reproductive damage in mice

CSE was prepared from commercial cigarettes, and CSE-HMF was then isolated using liquid-liquid extraction and Sephadex LH-20 column chromatography (Fig. 2A). The concentration of 5-HMF in the crude CSE was determined to be 2.01 ± 0.04 mg per cigarette. After 60 days of treatment, neither CSE nor CSE-HMF altered body weight, the relative weights of reproductive organs (Fig. S1A), or serum levels of sex hormones (T, E₂, FSH and LH) (Fig. S1B). However, both treatments significantly decreased sperm count, total motility, and progressive motility (Fig. 2B) and induced histopathological alterations, including dislodgment of immature germ cells, seminiferous epithelium vacuolization, and decreased density of germ cells (Fig. 2C). These findings identify 5-HMF as an important cytotoxic component in cigarette smoke that impairs spermatogenesis.

To confirm the specific role of 5-HMF, we treated mice with commercially sourced pure 5-HMF (Fig. 2D). As shown in Figs. 2E, 5-HMF levels were significantly elevated in the serum and testes after treatment, indicating that inhaled 5-HMF distributes to the testis in mice. Moreover, pure 5-HMF recapitulated the adverse effects observed with CSE-HMF, significantly reducing sperm count, total motility, and progressive motility (Fig. 2F) and causing identical testicular and epididymal damage (Fig. 2G). This consistency confirms that 5-HMF is the active component within CSE responsible for spermatogenic impairment.

3.2.1. HMF compromises the barrier function in the testis and isolated Sertoli cells in mice

Compared to the intact BTB with typical 'sandwich' structure in controls, 5-HMF treatment markedly disrupted the barrier integrity, characterized by vacuolization of Sertoli cells, barrier junction fragmentation, and diminished actin filament staining (Fig. 3A). Further, the distribution of the fluorescent biotin tracer after micro-injection was markedly different between groups. While it was strictly limited to the interstitial compartment in the testis of mice treated with saline, 5-HMF treatment resulted in its widespread diffusion into the seminiferous tubules (Fig. 3B). As shown in Figs. 3C, 5-HMF exposure significantly reduced the expression of TJ proteins (ZO-1, Occludin, Claudin-5, Claudin-11) in the mouse testis, while the levels of basal ectoplasmic specialization proteins (N-cadherin, α -catenin, β -catenin) were unaltered.

Isolated Sertoli cells with high purity (Fig. S2) were used to further validate the findings from the *in vivo* experiments. As shown in Fig. S3, 5-HMF decreased cell viability in a dose-dependent manner, with a significant reduction observed at concentrations of 100 μ M and above. Based on this dose-response relationship, concentrations of 10 μ M and 40 μ M, at which cell viability was not significantly altered, were chosen for subsequent experiments. The concentrations exceeded the measured average *in vivo* levels (serum: 370 ng/mL; testes: 280 ng/g), which is an expected and common practice given that cell culture systems lack systemic pharmacokinetics and often require higher doses to achieve a biological effect within a limited timeframe. As expected, 5-HMF treatment significantly reduced the protein levels of ZO-1, Occludin, Claudin-5, Claudin-11, and α -catenin in Sertoli cells (Fig. 3D). This reduction in TJ proteins did not correspond to transcriptional changes: mRNA levels of *zo-1*, *claudin-5*, and *claudin-11* were unaffected in both 5-HMF-treated mice and Sertoli cells (Fig. S4). The functional consequence of this TJ disruption was confirmed by a significant decrease in TER following treatment with 40 μ M 5-HMF, measured on days 7 and 8 (Fig. 3E). Taken together, these data indicate that 5-HMF compromises the integrity and function of the BTB.

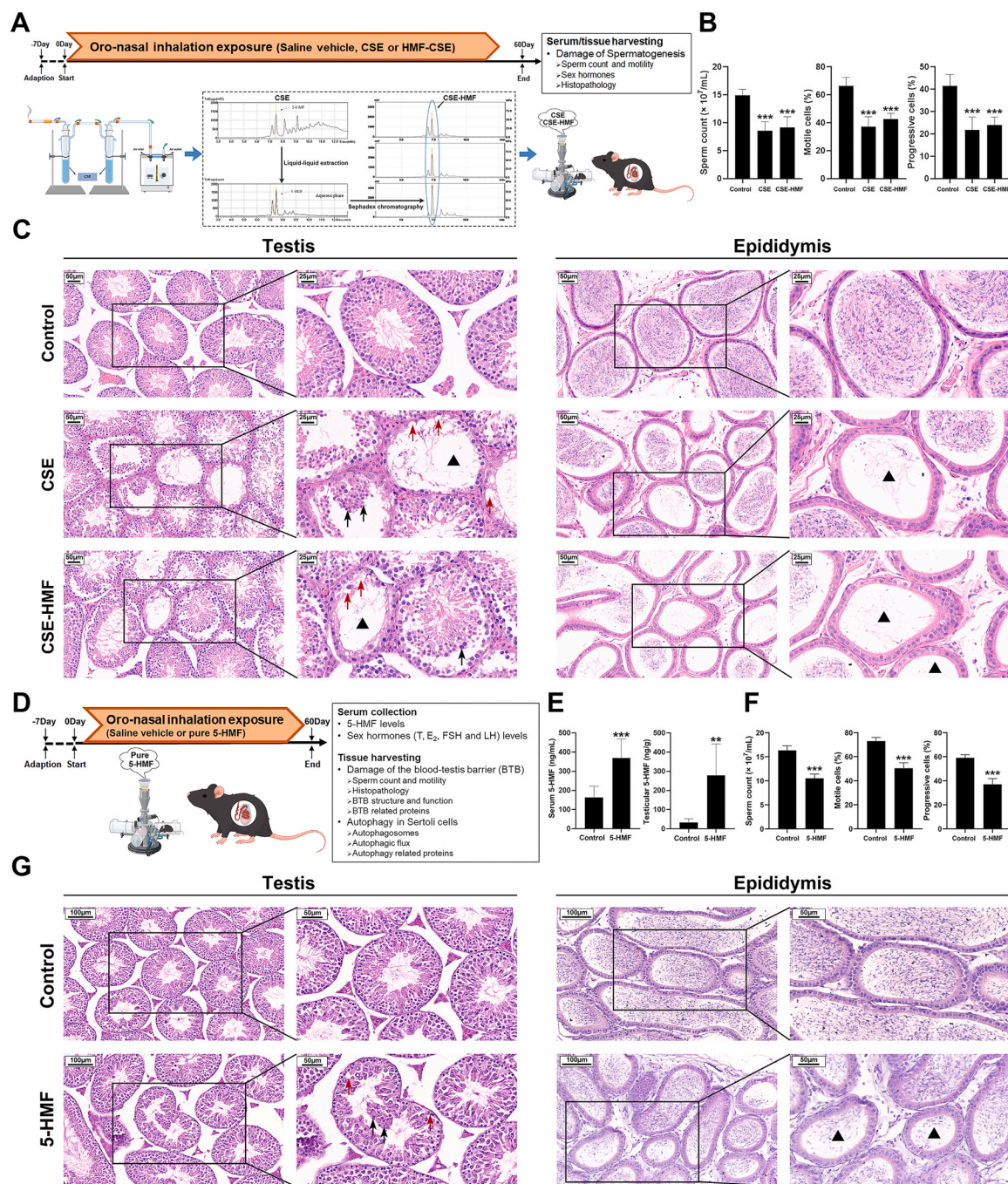


Fig. 2. 5-HMF as an important component in cigarette smoke induces male reproductive damage in mice. (A) Schematic diagram of the experimental design. CSE was prepared from commercial cigarettes, and a 5-HMF-enriched fraction (CSE-HMF) was isolated via liquid-liquid extraction and Sephadex LH-20 column chromatography. WT male mice ($n = 6$ per group) underwent nose-only inhalation exposure to aerosolized saline, CSE (equivalent to 20 cigarettes), or a volume-matched dose of CSE-HMF for 60 days prior to evaluation. (B) Sperm parameters (sperm count, total motility and progressive motility) in the mouse epididymis ($n = 6$ per group). (C) Representative H&E-stained sections of the testis and epididymis. Black arrow, dislocated immature germ cells; red arrow, vacuolar Sertoli cells; black triangle, decreased density of germ cells. Scale bars: 50 μm (left panel); 25 μm (right panel). (D) Schematic diagram of the *in vivo* administration of pure 5-HMF. WT male mice ($n = 7$ per group) underwent nose-only inhalation exposure to aerosolized saline, or pure 5-HMF (2 mg/mL) for 60 days prior to evaluation. (E) 5-HMF levels in mouse serum and testis ($n = 7$ per group). (F) Sperm parameters (sperm count, total motility and progressive motility) in the mouse epididymis ($n = 7$ per group). (G) Representative H&E-stained sections of the testis and epididymis. Black arrow, dislocated immature germ cells; red arrow, vacuolar Sertoli cells; black triangle, decreased density of germ cells. Scale bars: 100 μm (left panel); 50 μm (right panel). Data are expressed as mean \pm SD. ** $P < 0.01$, *** $P < 0.001$, compared with the control group.

3.2.2. HMF stimulates autophagic flux in the testis and isolated Sertoli cells in mice

TEM analysis revealed that 5-HMF induced the accumulation of both double-membrane autophagosomes and single-membrane autolysosomes in the testis and isolated Sertoli cells in mice (Fig. 4A-B).

Consistent with this finding, immunofluorescence analysis showed that 5-HMF significantly increased the number of LC3 puncta in Sertoli cells (Fig. 4 C). Since an increase in autophagosomes can reflect either enhanced formation or impaired degradation of autophagy, we next sought to distinguish between these possibilities to clarify the

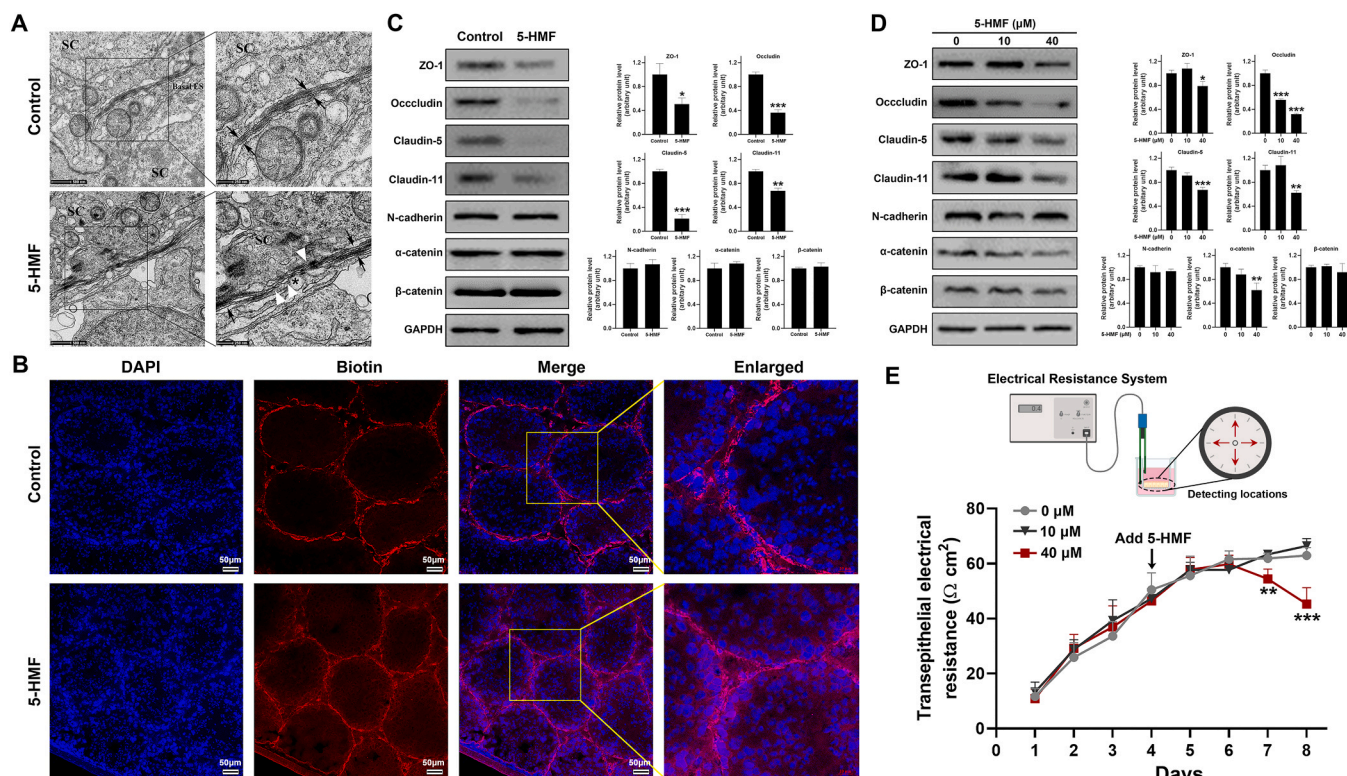


Fig. 3. 5-HMF compromises the barrier function in the testis and isolated Sertoli cells in mice. (A) Representative TEM images of mouse testis. SC, Sertoli cell; Basal ES, basal ectoplasmic specialization; black arrow, TJ; white triangle, disassembly of the TJ; black asterisk, vacuolization. Scale bar: 500 nm (left panel), 250 nm (right panel). (B) Representative confocal fluorescence images of the distribution of biotin tracer in mouse testis. Scale bars: 50 μm . (C–D) The expression of barrier junction-related proteins in the testis (C) and isolated Sertoli cells (D) ($n = 3$ per group) in mice. GAPDH was used as a protein loading control. Band intensity was quantified using ImageJ software. (E) Junctional permeability of isolated Sertoli cells treated with 5-HMF for the indicated time ($n = 4$ per group). Data are expressed as mean \pm SD. * $P < 0.05$, ** $P < 0.01$, *** $P < 0.001$, compared with the control group.

autophagic flux status. As shown in Figs. 4D, 5-HMF significantly decreased the protein levels of SQSTM1/p62, a selective autophagic substrate, in Sertoli cells, suggesting that autophagic flux was activated. This was further supported by the exacerbated accumulation of LC3-II in Sertoli cells co-treated with 5-HMF and CQ (Fig. 4E). Moreover, autophagic flux was also assessed using cells transfected with GFP-mRFP-LC3 lentivirus, wherein autophagosomes (yellow puncta) are distinguished from autolysosomes (red-only puncta) based on the pH-dependent quenching of GFP signal in acidic compartments, the number of both yellow puncta and red puncta was significantly increased following 5-HMF exposure (Fig. 4F). Collectively, these findings indicate that 5-HMF activates autophagic flux in Sertoli cells.

3.3. Pharmacological autophagy inhibition alleviates 5-HMF-induced BTB disassembly between Sertoli cells

To investigate the role of autophagy in 5-HMF-induced BTB disruption, we employed 3-MA (an early-stage autophagy inhibitor) and CQ (a late-stage autophagy blocker) in the subsequent rescue experiments. The results showed that both inhibitors significantly attenuated the 5-HMF-induced reduction in TER across Sertoli cell monolayers (Fig. 5A), indicating a functional recovery of the barrier. Concurrently, the downregulation of TJ proteins (ZO-1, Occludin, Claudin-5, and Claudin-11) caused by 5-HMF was markedly reversed by 3-MA and CQ treatment (Fig. 5B–C). Furthermore, immunofluorescence co-staining for LC3 and Occludin revealed that 5-HMF reduced membrane-localized Occludin while increasing the levels of LC3. This effect was reversed by 3-MA, which increased Occludin signals both at the membrane and within the cytoplasm (Fig. 5D). These results suggest that autophagy underlies the down-regulation of TJ proteins and subsequent BTB disruption

induced by 5-HMF.

3.3.1. HMF increases autophagic flux via mTOR-mediated Atg12 upregulation in the testis and isolated Sertoli cells in mice

Next, we investigated the underlying mechanisms by which 5-HMF enhances autophagic flux in Sertoli cells. The results of western blot analysis revealed that 5-HMF significantly decreased p-mTOR levels and up-regulated Atg12 both *in vivo* and in isolated Sertoli cells (Fig. 6A–B), suggesting that mTOR-mediated up-regulation of Atg12 may play a critical role in mediating 5-HMF-induced autophagy activation. To validate these findings, we generated an Atg12-knockout mouse model using CRISPR-Cas9 (Fig. S5A). Although *atg12*^{−/−} neonates were born with normal morphology, they exhibited complete neonatal lethality on postnatal day 1 (PND1). Western blot analysis confirmed the complete absence of Atg12 and LC3-II protein in *atg12*^{−/−} mice compared to WT controls. Moreover, *atg12*^{+/-} heterozygous mice exhibited protein levels of Atg12 and LC3-II that were intermediate between those of *atg12*^{−/−} and WT mice (Fig. 6C–D). Given the lethal phenotype of the homozygous knockout, the *atg12*^{+/-} mouse presents a viable and suitable model for further functional analysis of Atg12.

While global *atg12* haploinsufficiency (*atg12*^{+/-}) had no significant impact on mouse body weight, sperm parameters, or spermatogenesis compared to WT mice (Fig. S5B–E), it significantly reduced expression in the testis and isolated Sertoli cells (Fig. 6F–G). Consequently, Atg12 deficiency markedly reversed the 5-HMF-induced accumulation of autophagic vacuoles (autophagosomes and autolysosomes) in the Sertoli cells of mouse testis (Fig. 6E). Correspondingly, the 5-HMF-mediated upregulation of Atg12 and LC3-II was abrogated by Atg12 deficiency in both mouse testis and cultured primary Sertoli cells (Fig. 6F–G). Taken together, these results demonstrate that the mTOR-mediated Atg12

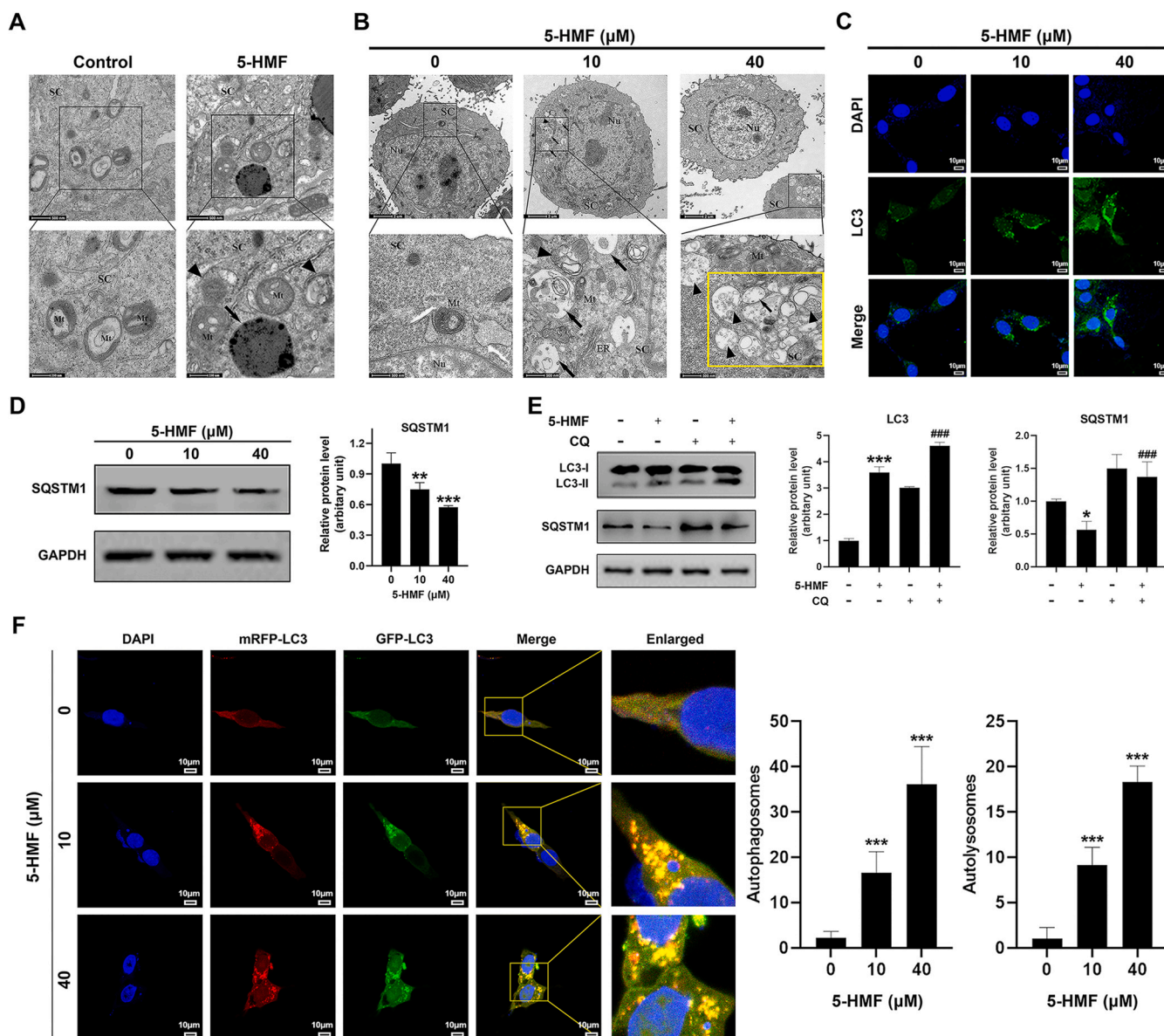


Fig. 4. 5-HMF stimulates autophagic flux in the testis and isolated Sertoli cells in mice. (A–B) Representative TEM images of mouse testis (A) and isolated Sertoli cells (B). SC, Sertoli cell; Mt, mitochondria; ER, endoplasmic reticulum; Nu, nuclear; black triangle, double-membrane autophagosome; black arrow, single-membrane autolysosome. Scale bars: 500 nm (top panel, testis); 250 nm (bottom panel, testis). Scale bars: 2 μm (top panel, isolated Sertoli cells); 500 nm (bottom panel, isolated Sertoli cells). (C) Representative confocal fluorescence images of LC3 (green) and DAPI (blue) in isolated Sertoli cells. Scale bar: 10 μm. (D–E) The expression of LC3 and SQSTM1 in isolated Sertoli cells treated with 5-HMF for 24 h in the presence or absence of CQ (n = 3 per group). GAPDH was used as a protein loading control. Band intensity was quantified using ImageJ software. (F) Representative confocal fluorescence images of TM4 cells transfected with GFP-mRFP-LC3 lentivirus. Scale bar: 10 μm. Data are expressed as mean ± SD. * $P < 0.05$, ** $P < 0.01$, *** $P < 0.001$, compared with the control group.

activation is a pivotal mechanism driving 5-HMF-induced autophagy.

3.4. *Atg12*-mediated autophagy activation contributes to 5-HMF-induced BTB disruption and male reproductive damage

Further, we explored if *Atg12* deficiency could prevent the 5-HMF-induced impairment of the BTB and the subsequent disruption of spermatogenesis. As shown in Fig. 7A, TEM analysis revealed that *Atg12* inhibition markedly ameliorated the 5-HMF-induced damage to the ultrastructure of the BTB, which was characterized by disrupted TJs and aberrant actin filament bundles between Sertoli cells. In addition, compared to WT mice treated with 5-HMF, less fluorescent biotin tracer diffused into the seminiferous tubules of *atg12*^{+/-} mice (Fig. 7B), indicating improved BTB integrity. Moreover, the 5-HMF-induced decrease

in the protein levels of ZO-1, Occludin, Claudin-5, and Claudin-11 in both WT mice and isolated Sertoli cells was significantly restored in the *atg12*^{+/-} groups (Fig. 7C–D). Consistently, 5-HMF-treated *atg12*^{+/-} Sertoli cells exhibited a marked increase in TER values compared to treated WT cells (Fig. 7E).

Consequently, *Atg12* deficiency significantly ameliorated the 5-HMF-induced impairment of sperm production and function, as shown by higher sperm counts, motility, and progression (Fig. 7F). This was accompanied by the attenuation of histopathological damages, including Sertoli cell vacuolization, seminiferous tubule disorganization, and reduced epididymal sperm density (Fig. 7G). Collectively, our results establish that 5-HMF impairs BTB integrity and function via *Atg12*-mediated autophagy activation, ultimately leading to disrupted spermatogenesis.

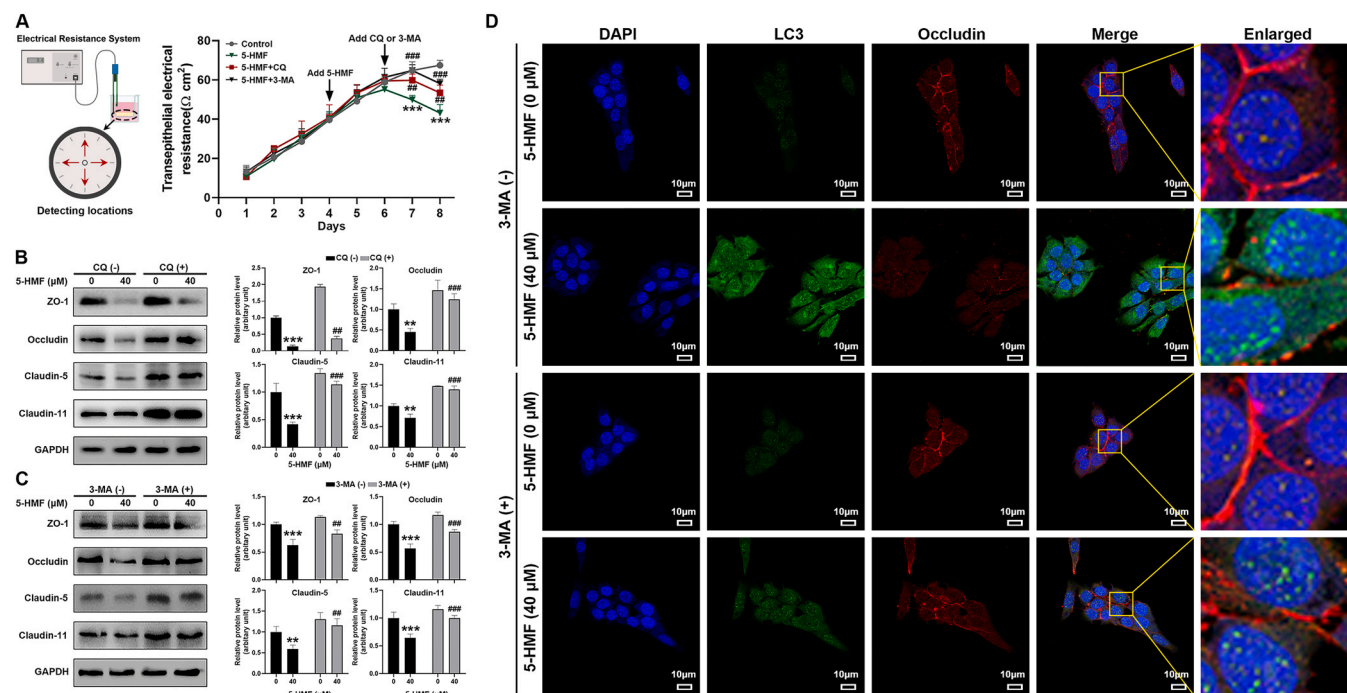


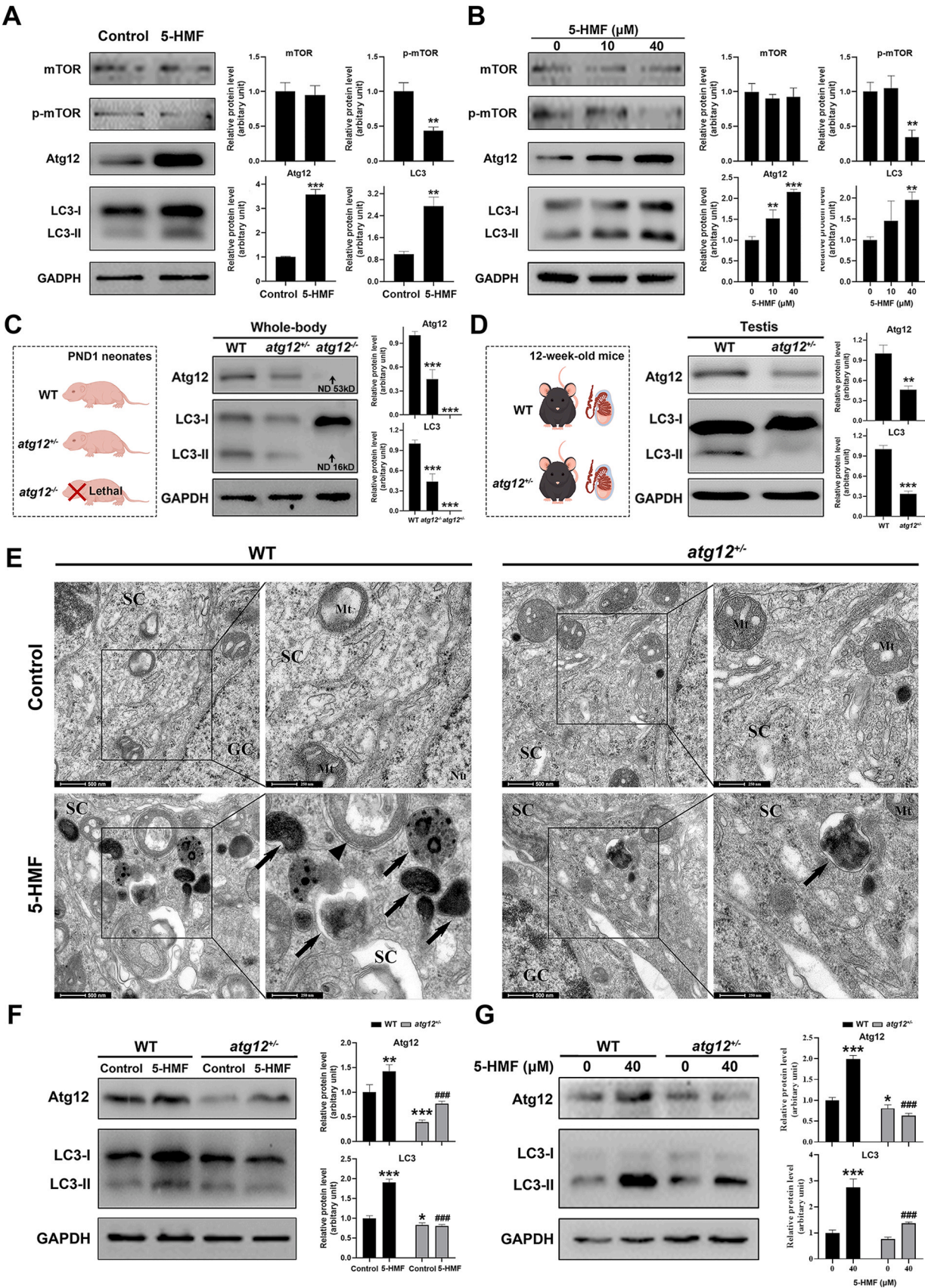
Fig. 5. Pharmacological autophagy inhibition alleviates 5-HMF-induced BTB disassembly between Sertoli cells. (A) Junctional permeability of isolated Sertoli cells treated with 5-HMF alone or in combination with CQ or 3-MA for the indicated time ($n = 4$ per group). (B-C) The expression of TJ-related proteins in isolated Sertoli cells treated with 5-HMF alone or in combination with CQ (B) or 3-MA (C) ($n = 3$ per group) for 24 h. GAPDH was used as a protein loading control. Band intensity was quantified using ImageJ software. (D) Representative confocal fluorescence images of LC3 (green), Occludin (red), and DAPI (blue) in isolated Sertoli cells. Scale bar: 10 μm . Data are expressed as mean \pm SD. $**P < 0.01$, $***P < 0.001$, compared with the control group; $\#P < 0.01$, $\###P < 0.001$, compared with the 5-HMF group.

4. Discussion

5-HMF is traditionally recognized as a processing contaminant in carbohydrate-rich foods such as dried fruits, cereals, bakery products, and roasted coffee (Abraham et al., 2011). Similarly, it is also a significant byproduct in cigarette smoke, due to the high carbohydrate content of tobacco leaves. During combustion, these carbohydrates undergo the Maillard reaction, generating 5-HMF along with other furfurals like furfural and 5-methylfurfural (Banožić et al., 2020; Ji et al., 2018). Therefore, smoking constitutes a direct and notable exposure pathway to 5-HMF, which is comparable in relevance to dietary exposure. However, epidemiological evidence linking cigarette smoking to 5-HMF exposure remains limited. Our study provides the first evidence that serum 5-HMF levels are significantly correlated with established biomarkers of cigarette smoke exposure (nicotine and cotinine). This correlation remained robust after adjustment for multiple potential confounders, including dietary intake. Critically, we found no significant difference in the consumption of major dietary sources of 5-HMF between smokers and non-smokers, which further argues against diet as a confounding factor. Despite this, dietary 5-HMF remains a major exposure source at the population level, given its widespread presence in thermally processed carbohydrate-rich foods and beverages, with concentrations reaching up to 2400 mg/kg in dried fruits, 1200 mg/L in coffee, 1655 mg/L in corn syrups, and 598 mg/L in wine (Martins et al., 2022). These substantial concentrations translate into a considerable daily dietary intake of 5-HMF, which in the European population is estimated to range from 67 to 170 $\mu\text{g/kg}$ per day (Abraham et al., 2011). However, since dietary 5-HMF can form low-toxicity adducts with cysteine in the gastrointestinal tract, its systemic health impact may be attenuated (Zhao et al., 2017). Therefore, our findings identify inhaled 5-HMF from cigarette smoke as an important toxicant that, by bypassing this intestinal detoxification, may directly contribute to smoking-related pathologies.

Accumulating epidemiological and experimental evidence has

established cigarette smoking as a modifiable risk factor for male reproductive damage (Corona et al., 2020). To further determine the role of 5-HMF in this process, we employed mouse models exposed to CSE, CSE-HMF, or pure 5-HMF. The daily 5-HMF dose (administered in both the pure and CSE-HMF groups) was calculated based on its detected yield per cigarette and scaled to simulate the exposure from 20 cigarettes daily. This regimen resulted in an average serum concentration of 370 ng/mL in mice, which was slightly lower than the average level reported in human smokers. The discrepancy may be attributed to additional dietary sources of 5-HMF (e.g., honey, dried fruits, and caramel) in humans versus the controlled diet of mice (Martins et al., 2022). Importantly, the fold increase was comparable between smokers/non-smokers (2.40) and 5-HMF/control mice (2.25), underscoring the translational relevance of our model. The results demonstrated that both CSE-HMF and 5-HMF elicited reproductive damage comparable to that induced by CSE, indicating that 5-HMF is an important contributor to the disruption of spermatogenesis caused by cigarette smoke. Furthermore, we found that 5-HMF accumulated in the testis without altering serum sex hormone levels, suggesting a direct testicular insult. Given that the BTB serves as the first line of defense against circulatory toxicants (Jiang et al., 2024a), we examined the impact of 5-HMF and found it disrupted BTB integrity and function. Mechanistically, this disruption may stem from the dysregulation of TJ proteins, as xenobiotic-induced BTB disruption often involves their downregulation and mislocalization. As reported, the neodymium oxide-induced activation of lncRNA SNHG5 down-regulated IGF2BP1 expression in Sertoli cells, thereby decreasing the stability of *occludin* mRNA and ultimately leading to BTB integrity disruption (Wang et al., 2024). Moreover, Yang et al. found that triptolide exposure disrupted BTB integrity through a specific downregulation of TJ proteins (ZO-1 and Claudin-11) that was mediated by the AKT/mTOR signaling pathway (Yang et al., 2024). Taken together, our findings support the hypothesis that 5-HMF, as an important cigarette smoke component, impairs



(caption on next page)

Fig. 6. 5-HMF increases autophagic flux via mTOR-mediated upregulation of Atg12 both in mouse testis and in isolated Sertoli cells. (A-B) The expression of autophagy-related proteins in the testis (A) and isolated Sertoli cells (B) ($n = 3$ per group). (C-D) The expression of Atg12 and LC3 in whole-body tissues of postnatal day 1 (PND1) mice (C) and in the testes of 12-week-old mice (D) across different genetic backgrounds (WT, *atg12*^{+/+} or *atg12*^{-/-}) ($n = 3$ per group). (E) Representative TEM images of testis from WT and *atg12*^{+/+} mice treated with 5-HMF. SC, Sertoli cell; GC, germ cell; Mt, mitochondria; black triangle, double-membrane autophagosome; black arrow, single-membrane autolysosome. Scale bar: 500 nm (left panel), 250 nm (right panel). (F-G) The expression of autophagy-related proteins in the testis (F) and isolated Sertoli cells (G) in WT and *atg12*^{+/+} mice treated with 5-HMF ($n = 3$ per group). GAPDH was used as a protein loading control. Band intensity was quantified using ImageJ software. Data are expressed as mean \pm SD. * $P < 0.05$, ** $P < 0.01$, *** $P < 0.001$, compared with the WT control group; ### $P < 0.001$, compared with the WT 5-HMF group.

spermatogenesis by disrupting the BTB via downregulation of TJ proteins.

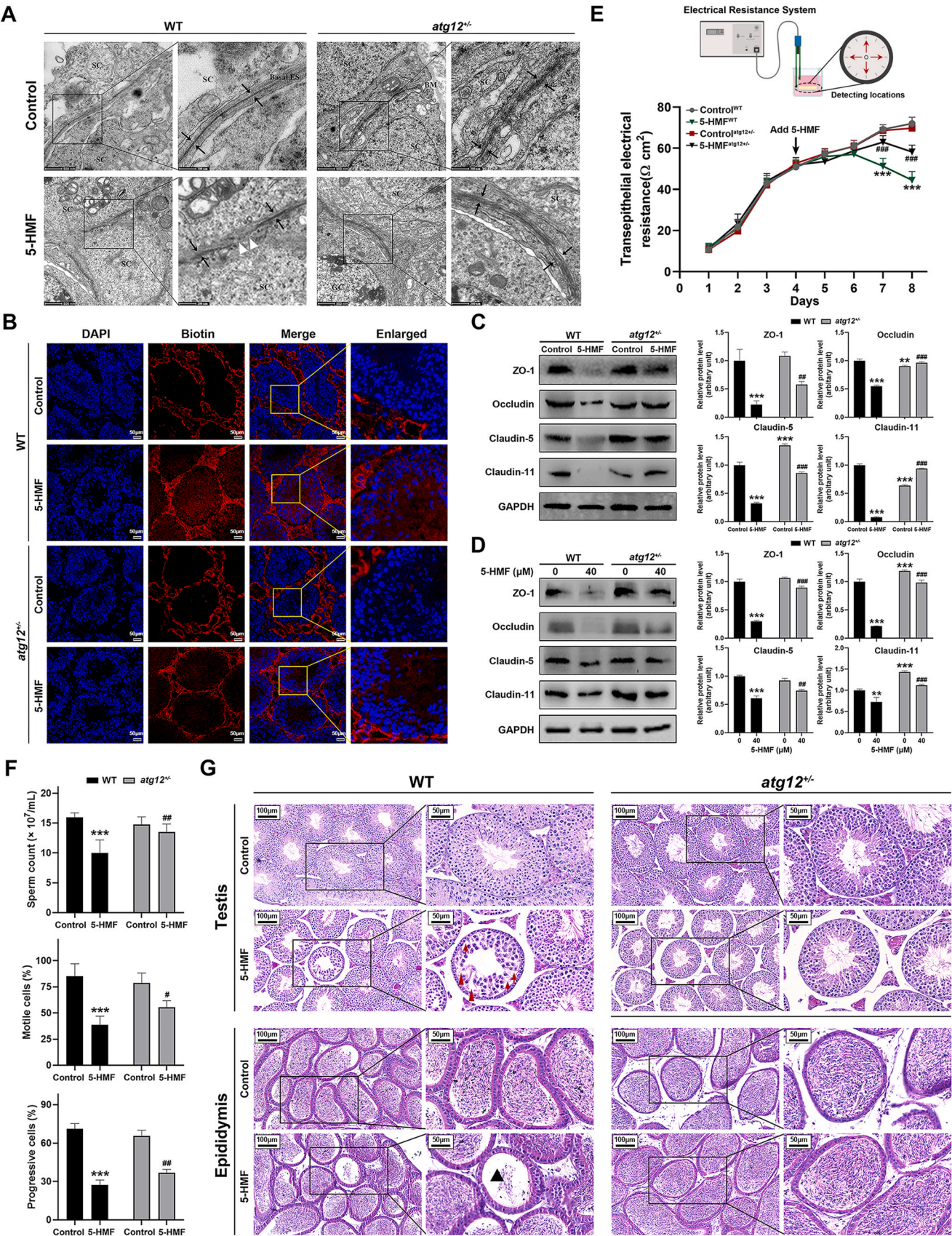
The BTB is a highly dynamic ultrastructure formed between Sertoli cells, undergoing continuous disassembly and reassembly during the seminiferous epithelial cycle (Luaces et al., 2023). This remodeling involves the endocytosis of TJ proteins via caveolin-1 or clathrin-mediated pathways, followed by autophagic degradation (Gehne et al., 2017). Given this context, we investigated whether 5-HMF impairs BTB integrity by activating autophagy and facilitating the degradation of TJ proteins. The results of TEM and LC3 immunofluorescence analyses revealed that 5-HMF significantly induced the accumulation of autophagosomes and autolysosomes in Sertoli cells. Since autophagosome accumulation can result from either increased formation or reduced clearance, we evaluated autophagic flux in response to 5-HMF. The level of SQSTM1, a protein degraded during autophagy, was decreased by 5-HMF treatment, suggesting enhanced autophagic activity. This was further supported by an increase in red-only puncta in mRFP-GFP-LC3 assays. Furthermore, we employed CQ to inhibit autolysosomal degradation in Sertoli cells. As expected, CQ co-treatment further increased LC3-II levels in 5-HMF-exposed cells, confirming that autophagy is activated following 5-HMF exposure. In rescue experiments, the 5-HMF-induced decrease in TER and TJ proteins was significantly reversed by inhibiting autophagy at both the early (with 3-MA) and late (with CQ) stages, underscoring the central role of autophagy in this process. In accordance with these findings, Xue et al. revealed that curcumin ameliorated aging-induced TJ damage and BTB disruption in Sertoli cells through its ability to suppress autophagy, an effect confirmed by CQ (Xue et al., 2025). Moreover, treatment with 10 μ M 5-HMF induced a slight but detectable increase in autophagic flux, as evidenced by TEM of Sertoli cells alongside LC3 immunofluorescence and western blot analyses of LC3 and SQSTM1. In contrast, the same treatment had minimal effects on TER and junction protein expression, with only Occludin showing a reduction. This indicates that autophagic activation is a more sensitive response to 5-HMF than junction disruption, and that mild autophagy does not compromise junctional integrity. Nevertheless, the mechanism underlying 5-HMF-induced autophagy activation is poorly understood.

mTOR is a serine-threonine protein kinase that is considered the master regulator of autophagy initiation. Suppression of mTOR is associated with enhanced autophagy (Gao et al., 2021). Our results also showed that 5-HMF exposure decreased the level of p-mTOR without altering the total mTOR protein level. This finding is consistent with a previous study reporting reduced p-mTOR levels in RAW 264.7 cells treated with 5-HMF (Kong et al., 2019). The inhibition of the mTOR pathway induced by 5-HMF may be associated with cellular oxidative stress. A recent study has demonstrated that 5-HMF can potentiate the Fenton reaction, leading to a dramatic, concentration-dependent increase in lipid peroxidation products and a depletion of antioxidant thiols (Greilberger et al., 2025). Given that oxidative stress serves as a critical upstream event to activate AMPK, and that activated AMPK can directly phosphorylate and inhibit the core components of mTORC1, thereby suppressing the mTOR signaling pathway (Cao et al., 2025), we propose that the inhibitory effect of 5-HMF on the mTOR pathway is mediated by oxidative stress mechanisms. Crucially, mTOR inactivation upregulates various ATG proteins (Li et al., 2025a); among them, Atg12 is critical for phagophore elongation and LC3 lipidation via the formation of the covalent Atg12-Atg5-Atg16L1 complex (Lystad et al., 2019).

Given the importance of these processes in autophagosome initiation and maturation, a previous study has shown that elevated Atg12 expression can lead to excessive autophagy activation, whereas genetic deletion of *atg12* inhibits autophagic flux (Malhotra et al., 2015). In the present study, we found that 5-HMF significantly upregulated Atg12 suggesting that Atg12 may play a central role in 5-HMF-induced autophagy activation. Consistently, it has been reported that xenobiotics, such as paraquat and ginsenoside Rg1, can enhance autophagy activity to exert downstream biological effects in an Atg12-dependent manner (Chen et al., 2024a; Huang et al., 2022). To further validate this hypothesis, we generated an Atg12 haploinsufficient mouse model (*atg12*^{+/+}). As expected, genetic reduction of Atg12 expression significantly attenuated 5-HMF-induced accumulation of autophagosomes and autolysosomes in the testis and isolated Sertoli cells in mice. Additionally, 5-HMF-induced increase in LC3-II levels was also suppressed by Atg12 deficiency. Collectively, these results indicate that 5-HMF-induced mTOR inhibition and Atg12 up-regulation is the culprit of autophagy activation in Sertoli cells.

Atg12-mediated autophagy is recognized as a key mechanism underlying the adverse effects of environmental toxicants on Sertoli cells and spermatogenesis. As reported, by up-regulating Atg12 proteins, microcystin-leucine arginine activated autophagy, leading to apoptosis in both the testis of zebrafish and TM4 cells (Wu et al., 2021). Moreover, the disruption of testicular function and differentiation by 4-nonylphenol exposure occurred through a mechanism involving the upregulation of Atg12 and subsequent stimulation of Sertoli cell autophagy (Duan et al., 2017). Supporting this, we found that 5-HMF-induced disruption of BTB integrity and function, primarily through the down-regulation of TJ proteins, was substantially rescued in *atg12*^{+/+} mice and isolated Sertoli cells. Consequently, 5-HMF-induced impairments in spermatogenesis were markedly ameliorated. Accordingly, our results suggest that activation of Atg12-mediated autophagy contributes to 5-HMF-induced BTB disruption and subsequent failure of spermatogenesis.

Despite providing novel insights into the reproductive toxicity of 5-HMF, this study has several limitations that should be noted. First, the nasal inhalation exposure model used in this study is a simplified paradigm. Compared to the active, deep inhalation of cigarette smoking, nasal exposure may lead to greater retention and local metabolism of 5-HMF in the nasal cavity (Ji et al., 2018), potentially reducing the dose reaching the deep lungs. Given the high absorption efficiency of the vast alveolar surface, our model could systematically underestimate the systemic exposure and toxicity of 5-HMF following deep pulmonary exposure. Therefore, our findings reflect the systemic effects specific to the intranasal route and should not be directly equated with the effects of cigarette smoking. Nevertheless, this model was appropriate for the core objective of this study: to assess the direct impact of inhaled 5-HMF, a key toxicant in cigarette smoke, on spermatogenesis and the BTB under controlled conditions, and to preliminarily elucidate its mechanisms. Second, while cigarette smoke is a complex mixture, this study specifically evaluated the effects of 5-HMF alone on spermatogenesis and BTB function to define its fundamental toxicological role; thus, coexposure experiments were not conducted. Previous studies suggest that components in cigarette smoke can interact with each other (Lin et al., 2025; Slotkin et al., 2019). However, potential synergistic or antagonistic interactions between 5-HMF and other smoke components remain to be investigated. This gap highlights the need to explore its broader health



(caption on next page)

Fig. 7. Atg12-mediated autophagy activation contributes to 5-HMF-induced BTB disruption. (A) Representative TEM images of testis in WT and *atg12*^{+/−} mice. SC, Sertoli cell; GC, germ cell; Basal ES, basal ectoplasmic specialization; BM, basement membrane; black arrow, TJs; white triangle, disassembly of the TJs. Scale bar: 500 nm (left panel), 250 nm (right panel). (B) Representative confocal fluorescence images of the distribution of biotin tracer in the testis of WT and *atg12*^{+/−} mice. Scale bars: 50 μ m. (C–D) The expression of TJ-related proteins in the testis (C) and isolated Sertoli cells (D) in WT and *atg12*^{+/−} mice (n = 3 per group). GAPDH was used as a protein loading control. Band intensity was quantified using ImageJ software. (E) Junctional permeability of isolated Sertoli cells of WT and *atg12*^{+/−} mice treated with 5-HMF for the indicated time (n = 4 per group). (F) Sperm parameters (sperm count, total motility and progressive motility) in the epididymis in WT and *atg12*^{+/−} mice (n = 6 per group). (G) Representative H&E-stained sections of the testis and epididymis in WT and *atg12*^{+/−} mice. Red arrow, vacuolar Sertoli cells; black triangle, decreased density of germ cells. Scale bars: 100 μ m (left panel); 50 μ m (right panel). Data are expressed as mean \pm SD. ***P* < 0.01, ****P* < 0.001, compared with the WT control group; #*P* < 0.05, ##*P* < 0.01, ###*P* < 0.001, compared with the WT 5-HMF group.

impacts and coexposure risks. Third, this study is limited by the use of *atg12*^{+/−} mice, necessitated by the embryonic lethality of the homozygous knockout. While this model provides valuable insight into haploinsufficiency, it precludes analysis of the complete loss-of-function phenotype that could reveal more profound biological effects. Therefore, employing Sertoli cell-specific conditional knockout models will be essential for future work to definitively establish the cell-autonomous role of Atg12.

5. Conclusion

In summary, our study provides the first evidence linking cigarette smoking to elevated serum 5-HMF levels and identifies 5-HMF as one of the important toxic components of cigarette smoke. This role was further substantiated using mouse models exposed to CSE and a 5-HMF-enriched fraction derived from CSE. Mechanistically, our findings indicate that 5-HMF decreases p-mTOR levels and upregulates Atg12 to activate autophagic flux, which subsequently decreases TJ protein expression, disrupts BTB integrity, and ultimately impairs spermatogenesis. Our findings identify autophagy as a key regulator of BTB integrity and function through its effects on TJ proteins, providing insights into the role of 5-HMF in cigarette smoke-induced disruption of spermatogenesis. Moreover, while the direct impact of dietary 5-HMF on mTOR signaling and the subsequent TJ disruption in Sertoli cells was not assessed in this study, our discovery that inhaled 5-HMF disrupts TJs, inhibits mTOR and activates autophagy, suggests a potential mechanism. Given the high concentrations of 5-HMF in many thermally processed foods, it is plausible that high oral intake could similarly compromise the BTB, a hypothesis that merits direct investigation in future studies.

CRedit authorship contribution statement

Shou-Lin Wang: Writing – review & editing, Supervision, Funding acquisition, Conceptualization. **Yongquan Yu:** Writing – original draft, Investigation, Funding acquisition, Conceptualization. **Mengfan Peng:** Methodology, Data curation. **Liu Yang:** Validation, Methodology. **Mingxiu Duan:** Methodology, Data curation. **Shuyu Xu:** Validation, Methodology. **Rong Xia:** Methodology. **Li Wang:** Formal analysis. **Shushu Li:** Visualization, Software, Resources. **Lifeng Tan:** Supervision, Resources, Project administration.

Declaration of Competing Interest

The authors declare that they have no known competing financial interests or personal relationships that could have appeared to influence the work reported in this paper.

Acknowledgments

This work was supported by the National Natural Science Foundation of China [82003494, 82173562, and 91743205] and the key projects of Changzhou Medical Center of Nanjing Medical University [CMCM202315]. We acknowledge BioRender for offering scientific illustration resources

Appendix A. Supporting information

Supplementary data associated with this article can be found in the online version at [doi:10.1016/j.ecoenv.2026.119825](https://doi.org/10.1016/j.ecoenv.2026.119825).

Data availability

Data will be made available on request.

References

- Abraham, K., Gürtler, R., Berg, K., Heinemeyer, G., Lampen, A., Appel, K.E., 2011. Toxicology and risk assessment of 5-Hydroxymethylfurfural in food. *Mol. Nutr. Food Res.* 55, 667–678. <https://doi.org/10.1002/mnfr.201000564>.
- Aktaş, I.G., Gökmen, V., 2021. Investigations on the formation of α -dicarbonyl compounds and 5-hydroxymethylfurfural in fruit products during storage: new insights into the role of Maillard reaction. *Food Chem.* 363, 130280. <https://doi.org/10.1016/j.foodchem.2021.130280>.
- Aydın, Y., Sarılioğlu, I., Armut, G., Calmaz, E., Orta Yılmaz, B., 2025. 5-Hydroxymethylfurfural causes reproductive toxicity in male mice by increasing oxidative stress and apoptosis through the Nrf2/HO-1 signaling pathway. *Toxicol. Mech. Methods* 28, 1–17. <https://doi.org/10.1080/15376516.2025.2537319>.
- Banožić, M., Jokić, S., Ackar, D., Blažić, M., Subarić, D., 2020. Carbohydrates-key players in tobacco aroma formation and quality determination. *Molecules* 25 1734. <https://doi.org/10.3390/molecules25071734>.
- Bao, M., Joza, P., Rickert, W.S., Lauterbach, J.H., 2010. An improved headspace solid-phase microextraction method for the analysis of free-base nicotine in particulate phase of mainstream cigarette smoke. *Anal. Chim. Acta* 663, 49–54. <https://doi.org/10.1016/j.aca.2010.01.036>.
- Boeri, L., Capogrosso, P., Ventimiglia, E., Pederzoli, F., Cazzaniga, W., Chierigo, F., Dehò, F., Montanari, E., Montorsi, F., Salonia, A., 2019. Heavy cigarette smoking and alcohol consumption are associated with impaired sperm parameters in primary infertile men. *Asian J. Androl.* 21, 478–485. https://doi.org/10.4103/aja.aja_110_18.
- Cao, Z., Huang, W., Sun, Y., Li, Y., 2020. Deoxynivalenol induced spermatogenesis disorder by blood-testis barrier disruption associated with testosterone deficiency and inflammation in mice. *Environ. Pollut.* 264, 114748. <https://doi.org/10.1016/j.envpol.2020.114748>.
- Cao, W., Liu, S., Zhang, L., Fu, X., Li, H., Ye, F., Bei, J., Ren, C., Ni, Y., Zhu, J., Wang, L., 2025. Therapeutic strategies in traditional Chinese medicine for premature ovarian failure: modulation of oxidative stress and autophagy-apoptosis via the AMPK/mTOR pathway. *Biosci. Trends* 19, 545–556. <https://doi.org/10.5582/bst.2025.01193>.
- Chen, Z., Chen, Z., Gao, S., Shi, J., Li, X., Sun, F., 2024b. PFOS exposure destroys the integrity of the blood-testis barrier (BTB) through PI3K/AKT/mTOR-mediated autophagy. *Reprod. Biol.* 24, 100846. <https://doi.org/10.1016/j.repbio.2023.100846>.
- Chen, N., Hu, H., Tang, J., Zheng, F., Guo, Z., Lin, X., Aschner, M., Shao, W., Yu, G., Cai, P., Chou, W.C., Wu, S., Li, H., 2024a. LncRNA NR_030777 promotes mitophagy by targeting CDK1-related mitochondrial fission and ATG12 to attenuate paraquat-induced Parkinson's disease. *Environ. Pollut.* 349, 123875. <https://doi.org/10.1016/j.envpol.2024.123875>.
- Cheng, C.Y., Mruk, D.D., 2012. The blood-testis barrier and its implications for male contraception. *Pharm. Rev.* 64, 16–64. <https://doi.org/10.1124/pr.110.002790>.
- Corona, G., Sansone, A., Pallotti, F., Ferlin, A., Pivonello, R., Isidori, A.M., Maggi, M., Jannini, E.A., 2020. People smoke for nicotine, but lose sexual and reproductive health for tar: a narrative review on the effect of cigarette smoking on male sexuality and reproduction. *J. Endocrinol. Invest.* 43, 1391–1408. <https://doi.org/10.1007/s40618-020-01257-x>.
- De Brucker, S., Dhooze, E., Drakopoulos, P., Uvin, V., Mackens, S., Boudry, L., De Vos, M., Vloeberghs, V., Tournaye, H., De Brucker, M., 2025. The influence of male smoking on success rates after IVF/ICSI. *Gynecol. Endocrinol.* 41, 2465594. <https://doi.org/10.1080/09513590.2025.2465594>.
- Duan, P., Hu, C., Quan, C., Yu, T., Huang, W., Chen, W., Tang, S., Shi, Y., Martin, F.L., Yang, K., 2017. 4-Nonylphenol induces autophagy and attenuates mTOR-p70S6K/4EBP1 signaling by modulating AMPK activation in Sertoli cells. *Toxicol. Lett.* 267, 21–31. <https://doi.org/10.1016/j.toxlet.2016.12.015>.
- Esakky, P., Hansen, D.A., Drury, A.M., Felder, P., Cusumano, A., Moley, K.H., 2018. Testicular cells exhibit similar molecular responses to cigarette smoke condensate ex vivo and in vivo. *Faseb J.* 32, 63–72. <https://doi.org/10.1096/fj.201700405R>.

- Gao, X., Yu, M., Sun, W., Han, Y., Yang, J., Lu, X., Jin, C., Wu, S., Cai, Y., 2021. Lanthanum chloride induces autophagy in primary cultured rat cortical neurons through Akt/mTOR and AMPK/mTOR signaling pathways. *Food Chem. Toxicol.* 158, 112632. <https://doi.org/10.1016/j.fct.2021.112632>.
- Gehne, N., Lamik, A., Lehmann, M., Haseloff, R.F., Andjelkovic, A.V., Blasig, I.E., 2017. Cross-over endocytosis of claudins is mediated by interactions via their extracellular loops. *PLoS One* 12, e0182106. <https://doi.org/10.1371/journal.pone.0182106>.
- Greilberger, J., Feigl, G., Greilberger, M., Bystrianska, S., Greilberger, M., 2025. 5-Hydroxymethylfurfural: A Particularly Harmful Molecule Inducing Toxic Lipids and Proteins? *Molecules* 30, 3897. <https://doi.org/10.3390/molecules30193897>.
- Gutvirtz, G., Sheiner, E., 2022. Airway pollution and smoking in reproductive health. *Best. Pr. Res. Clin. Obstet. Gynaecol.* 85, 81–93. <https://doi.org/10.1016/j.bpobgyn.2022.09.005>.
- Hermundsgård, D.H., Ghoreishi, S., Tanase-Opedal, M., Moe, S.T., Brusletto, R., Barth, T., 2025. Maximizing yields of furfural and 5-hydroxymethylfurfural in side streams from steam explosion of lignocellulosic residues. *Biofuels Bioprod. Bioref.* 19, 319–336. <https://doi.org/10.1002/bbb.2719>.
- Huang, C., Xue, X., Gong, N., Jiang, J., 2022. Ginsenoside Rg1 suppresses paraquat-induced epithelial cell senescence by enhancing autophagy in an ATG12-dependent manner. *Environ. Toxicol.* 37, 2302–2313. <https://doi.org/10.1002/tox.23597>.
- Ji, M., Zhang, Z., Li, N., Xia, R., Wang, C., Yu, Y., Yao, S., Shen, J., Wang, S.L., 2018. Identification of 5-hydroxymethylfurfural in cigarette smoke extract as a new substrate metabolically activated by human cytochrome P450 2A13. *Toxicol. Appl. Pharm.* 359, 108–117. <https://doi.org/10.1016/j.taap.2018.09.031>.
- Jiang, J., Shu, Z., Qiu, L., 2024b. Adverse effects and potential mechanisms of polystyrene microplastics (PS-MPs) on the blood-testis barrier. *Environ. Geochem. Health* 46, 238. <https://doi.org/10.1007/s10653-024-02033-z>.
- Jiang, B., Yang, D., Peng, H., 2024a. Environmental toxins and reproductive health: unraveling the effects on Sertoli cells and the blood-testis barrier in animals. *Biol. Reprod.* 111, 977–986. <https://doi.org/10.1093/biolre/iaoe126>.
- Karlsson, O., Torniainen, P., Dagbro, O., Granlund, K., Morén, T., 2012. Presence of water-soluble compounds in thermally modified wood: Carbohydrates and furfurals. *Bioresources* 7, 3679–3689. <https://doi.org/10.4067/S0718-221X2012000200010>.
- Kong, F., Lee, B.H., Wei, K., 2019. 5-Hydroxymethylfurfural Mitigates Lipopolysaccharide-Stimulated Inflammation via Suppression of MAPK, NF- κ B and mTOR Activation in RAW 264.7 Cells. *Molecules* 24, 275. <https://doi.org/10.3390/molecules24020275>.
- Kulaksiz, D., Toprak, T., Tokat, E., Yilmaz, M., Ramazanoglu, M.A., Garayev, A., Sulukaya, M., Degirmenetepe, R.B., Allahverdiyev, E., Gul, M., Verit, A., 2022. Sperm concentration and semen volume increase after smoking cessation in infertile men. *Int. J. Impot Res* 34, 614–619. <https://doi.org/10.1038/s41443-022-00605-0>.
- La Maestra, S., De Flora, S., Micale, R.T., 2015. Effect of cigarette smoke on DNA damage, oxidative stress, and morphological alterations in mouse testis and spermatozoa. *Int. J. Hyg. Environ. Health* 218, 117–122. <https://doi.org/10.1016/j.ijheh.2014.08.006>.
- Li, S., Xia, R., Gong, X., Wang, C., Liu, H., Dong, H., Su, Z., Liang, Y., Wang, S., Yang, T., 2025b. Mediating effect of TyG index on the association between glucose-lipid metabolism-related dietary pattern and T2DM: a propensity score-matched analysis. *BMC Endocr. Disord.* 25, 114. <https://doi.org/10.1186/s12902-025-01892-6>.
- Li, J., Zhang, D., Liu, P., Fang, R., Li, Y., Zhu, Y., Dong, M., Xie, S., Liu, Y., Wu, J., Zhu, G., Han, J., 2025a. Licochalcone A promotes autophagy to ameliorate NAFLD by inhibiting the mTOR and regulating ULK1/Beclin1/VPS34 pathway. *J. Ethnopharmacol.* 29, 120333. <https://doi.org/10.1016/j.jep.2025.120333>.
- Liang, Q., Liu, B.Y., Zhang, T.L., Zhang, H.J., Ren, Y.L., Wang, H.P., Wang, H., Wang, L., 2024. Chronic dietary exposure to glyphosate-induced connexin 43 autophagic degradation contributes to blood-testis barrier disruption in roosters. *Sci. Total Environ.* 951, 175606. <https://doi.org/10.1016/j.scitotenv.2024.175606>.
- Lin, H., Li, Z., Zeng, T., Wang, Y., Zhang, L., 2025. The crucial involvement of gamma-Mangostin and CYP1B1 in the mechanism underlying the toxicity caused by cigarette smoke extract: In silico and in vitro insights. *Toxicology* 510, 154016. <https://doi.org/10.1016/j.tox.2024.154016>.
- Luaces, J.P., Toro-Urrego, N., Otero-Losada, M., Capani, F., 2023. What do we know about blood-testis barrier? current understanding of its structure and physiology. *Front Cell Dev. Biol.* 11, 1114769. <https://doi.org/10.3389/fcell.2023.1114769>.
- Lystad, A.H., Carlsson, S.R., Simonsen, A., 2019. Toward the function of mammalian ATG12-ATG5-ATG16L1 complex in autophagy and related processes. *Autophagy* 15, 1485–1486. <https://doi.org/10.1080/15548627.2019.1618100>.
- Malhotra, R., Warne, J.P., Salas, E., Xu, A.W., Debnath, J., 2015. Loss of Atg12, but not Atg5, in pro-opiomelanocortin neurons exacerbates diet-induced obesity. *Autophagy* 11, 145–154. <https://doi.org/10.1080/15548627.2014.998917>.
- Martins, F., Alcantara, G., Silva, A.F.S., Melchert, W.R., Rocha, F.R.P., 2022. The role of 5-hydroxymethylfurfural in food and recent advances in analytical methods. *Food Chem.* 395, 133539. <https://doi.org/10.1016/j.foodchem.2022.133539>.
- Mruk, D.D., Cheng, C.Y., 2015. The Mammalian Blood-Testis Barrier: Its Biology and Regulation. *Endocr. Rev.* 36, 564–591. <https://doi.org/10.1210/er.2015-1127>.
- Orta Yilmaz, B., Aydin, Y., 2024. New insights into the mechanisms underlying 5-hydroxymethylfurfural-induced suppression of testosterone biosynthesis in vivo and in vitro. *Toxicol. Appl. Pharm.* 493, 117142. <https://doi.org/10.1016/j.taap.2024.117142>.
- Peña-Corona, S.I., Vargas-Estrada, D., Juárez-Rodríguez, I., Retana-Márquez, S., Mendoza-Rodríguez, C.A., 2023. Bisphenols as promoters of the dysregulation of cellular junction proteins of the blood-testis barrier in experimental animals: a systematic review of the literature. *J. Biochem. Mol. Toxicol.* 37, e23416. <https://doi.org/10.1002/jbt.23416>.
- Qiu, L., Zhang, X., Zhang, X., Zhang, Y., Gu, J., Chen, M., Zhang, Z., Wang, X., Wang, S.L., 2013. Sertoli cell is a potential target for perfluorooctane sulfonate-induced reproductive dysfunction in male mice. *Toxicol. Sci.* 135, 229–240. <https://doi.org/10.1093/toxsci/kft129>.
- Radbel, J., Rebuli, M.E., Kipen, H., Brigham, E., 2024. Indoor air pollution and airway health. *J. Allergy Clin. Immunol.* 154, 835–846. <https://doi.org/10.1016/j.jaci.2024.08.013>.
- Rahban, R., Nef, S., 2020. Regional difference in semen quality of young men: a review on the implication of environmental and lifestyle factors during fetal life and adulthood. *Basic Clin. Androl.* 30, 16. <https://doi.org/10.1186/s12610-020-00114-4>.
- Rigotti, N.A., Kruse, G.R., Livingstone-Banks, J., Hartmann-Boyce, J., 2022. Treatment of tobacco smoking: a review. *Jama* 327, 566–577. <https://doi.org/10.1001/jama.2022.0395>.
- Rotimi, D.E., Singh, S.K., 2024. Implications of lifestyle factors on male reproductive health. *JBRA Assist. Reprod.* 28, 320–330. <https://doi.org/10.5935/1518-0557.20240007>.
- Saewu, A., Kongmanas, K., Raghupathy, R., Netherton, J., Kadunganattil, S., Linton, J.J., Chaisuriyong, W., Faull, K.F., Baker, M.A., Tanphaichitr, N., 2020. Primary sertoli cell cultures from adult mice have different properties compared with those derived from 20-day-old animals. *Endocrinology* 161, bqz020. <https://doi.org/10.1210/endo/bqz020>.
- Sharma, R., Harlev, A., Agarwal, A., Esteves, S.C., 2016. Cigarette smoking and semen quality: a new meta-analysis examining the effect of the 2010 world health organization laboratory methods for the examination of human semen. *Eur. Urol.* 70, 635–645. <https://doi.org/10.1016/j.eururo.2016.04.010>.
- Slotkin, T.A., Skavicus, S., Ko, A., Levin, E.D., Seidler, F.J., 2019. The developmental neurotoxicity of tobacco smoke can be mimicked by a combination of nicotine and Benzo[a]Pyrene: effects on cholinergic and serotonergic systems. *Toxicol. Sci.* 167, 293–304. <https://doi.org/10.1093/toxsci/kfy241>.
- Wang, S., Ma, Y., Li, W., Zhao, Y., Gao, Y., Wang, S., 2024. LncRNA SNHG5/IGF2BP1/Occludin axis regulates Nd(2)O(3) induced blood-testis barrier disruption. *Environ. Pollut.* 358, 124527. <https://doi.org/10.1016/j.envpol.2024.124527>.
- Wang, Q., Su, Y., Yang, Q., Beta, T., Shen, F., Liu, Q., 2025. EGCG attenuates BPA-induced male reproductive toxicity by regulating the blood-testis barrier by suppressing autophagy via AMPK/AKT/mTOR signaling pathway. *Comp. Biochem. Physiol. C. Toxicol. Pharm.* 297, 110298. <https://doi.org/10.1016/j.cbpc.2025.110298>.
- Wu, Z., Wang, F., Hu, L., Zhang, J., Chen, D., Zhao, S., 2021. Inhibition of endoplasmic reticulum stress-related autophagy attenuates MCLR-induced apoptosis in zebrafish testis and mouse TM4 cells. *Ecotoxicol. Environ. Saf.* 221, 112438. <https://doi.org/10.1016/j.ecoenv.2021.112438>.
- Wu, X., Yang, J., Liao, J., Zalán, Z., Kan, J., Suo, H., Zhang, Y., Song, J., 2025. Identification of critical gut metabolites mediating the protective effects of lacticaseibacillus paracasei on myocardial injury in mice. *J. Agric. Food Chem.* 73, 18822–18840. <https://doi.org/10.1021/acs.jafc.5c08360>.
- Xia, Y., Hao, L., Li, Y., Li, Y., Chen, J., Li, L., Han, X., Liu, Y., Wang, X., Li, D., 2023. Embryonic 6:2 FTOH exposure causes reproductive toxicity by disrupting the formation of the blood-testis barrier in offspring mice. *Ecotoxicol. Environ. Saf.* 250, 114497. <https://doi.org/10.1016/j.ecoenv.2023.114497>.
- Xue, C., Yan, Z., Cheng, W., Zhang, D., Zhang, R., Duan, H., Zhang, L., Ma, X., Hu, J., Kang, J., Ma, X., 2025. Curcumin ameliorates aging-induced blood-testis barrier disruption by regulating AMPK/mTOR mediated autophagy. *PLoS One* 20, e0321752. <https://doi.org/10.1371/journal.pone.0321752>.
- Yan, Q., Zhang, Y., Wang, Q., Yuan, L., 2022. Autophagy: A Double-Edged Sword in Male Reproduction. *Int. J. Mol. Sci.* 23, 15273. <https://doi.org/10.3390/ijms232315273>.
- Yang, X., He, L., Li, X., Wang, L., Bu, T., Yun, D., Lu, X., Gao, S., Huang, Q., Li, J., Zheng, B., Yu, J., Sun, F., 2024. Triptolide exposure triggers testicular vacuolization injury by disrupting the Sertoli cell junction and cytoskeletal organization via the AKT/mTOR signaling pathway. *Ecotoxicol. Environ. Saf.* 279, 116502. <https://doi.org/10.1016/j.ecoenv.2024.116502>.
- Zhang, J., Bai, R., Yi, X., Yang, Z., Liu, X., Zhou, J., Liang, W., 2016. Fully automated analysis of four tobacco-specific N-nitrosamines in mainstream cigarette smoke using two-dimensional online solid phase extraction combined with liquid chromatography-tandem mass spectrometry. *Talanta* 146, 216–224. <https://doi.org/10.1016/j.talanta.2015.08.057>.
- Zhao, Q., Zou, Y., Huang, C., Lan, P., Zheng, J., Ou, S., 2017. Formation of a Hydroxymethylfurfural-Cysteine Adduct and Its Absorption and Cytotoxicity in Caco-2 Cells. *J. Agric. Food Chem.* 65, 9902–9908. <https://doi.org/10.1021/acs.jafc.7b03938>.
- Zheng, S., Jiang, L., Qiu, L., 2024. The effects of fine particulate matter on the blood-testis barrier and its potential mechanisms. *Rev. Environ. Health* 39, 233–249. <https://doi.org/10.1515/reveh-2022-0204>.